1969

# Resolution limitations in medical ultrasonics

Russell Lee Pimmel
*Iowa State University*

# RESOLUTION LIMITATIONS IN MEDICAL ULTRASONICS

by

Russell Leo Pimmel

A Dissertation Submitted to the
Graduate Faculty in Partial Fulfillment of
The Requirements for the Degree of
DOCTOR OF PHILOSOPHY

Major Subject: Electrical Engineering

Approved:

Signature was redacted for privacy.

In Charge of Major Work

Signature was redacted for privacy.

Head of Major Department

Signature was redacted for privacy.

Dean of Graduate College

Iowa State University
Ames, Iowa

1969

# TABLE OF CONTENTS

# INTRODUCTION

Sound is a form of mechanical energy propagated as a disturbance in a supportive media. By definition, sound of a frequency greater than 20 KC is called ultrasound.

Diagnostic ultrasonics is a general term describing the utilization of ultrasonic energy to obtain information useful in classifying invisible features. The technique has its origin in the flaw detection systems developed to locate imperfection in metal castings. It has been extended to include medical diagnosis, with the visualization of the internal organs one of the primary applications. Among the organs examined are the brain (16, 30, 39), eye (2, 34), thyroid (7, 14), breast (32, 41), bladder (21), heart (1, 9, 23), liver (20), kidney (21, 29), spleen (28), and uterus (27, 32).

## General Technique

For diagnostic ultrasonics, the technique is essentially one of echo-ranging. A pulse of sonic energy is transmitted into the body from a crystal which produces a short burst of sonic energy when excited electrically. The sound is formed into a narrow beam determined by the size and shape of the transducer crystal. Each discontinuity in the acoustical properties of the tissue produces an echo which is detected by the receiver. From the position and orientation of the

transducer, the time between transmitted and received pulses, and the velocity of sound, each discontinuity is located. This "computation" is done electronically in real time, and these bits of information are combined either on a cathode ray tube or on photographic film to give a "line" picture of the discontinuities, which is called a "sonogram".

## Advantage of Diagnostic Ultrasonics

Since sonograms resemble images obtained by x-rays and other radiological techniques, the question arises, "Why ultrasonics?" First, ultrasonic examination provides diagnostic information that is not readily available by other techniques. The point of view is different; the sonogram is a cross sectional picture, while the x-ray is a projected view. Sensitivity of the sonic technique to slight changes in the tissue properties allows visualization without the use of a contrast media often required in radiological examinations. Secondly, the ultrasonic technique is much safer since ultrasound does not produce the cellular damage associated with radiation. Frictional heating is the only cellular effect of sonic energy, and power levels used in diagnostic work provide an extremely safe margin since they are 1/1000 of those used in physical therapy for heating deep muscles (19, p. 60).

## Disadvantage of Diagnostic Ultrasonics

Diagnostic ultrasound has some serious shortcomings. A significant portion of the sonic energy is reflected at the interface formed by a gas and a liquid or solid. To obtain a reasonable signal-noise relationship at the transducer a liquid coupler between the transducer and the skin is necessary; either a water bath or an oil film is used. To use water as transmitting media, both the transducer and the region of the body to be examined are immersed in the bath, resulting in some obvious problems, particularly when examining the critically ill or the subject's facial area. In using the latter method, some difficulty occurs in keeping track of the transducer location and orientation.

Radiological methods utilize a direct technique; in making an x-ray, the patient is placed between the source of energy and recording film. In contrast, the sonogram is produced by an echo technique in which each bit of information is sequentially obtained and then combined to form the image. There are many inherent limitations with this type of visualization, particularly in locating and describing the echo producing interfaces.

In diagnostic ultrasonics, three variables are generally determined in generating the sonogram. Two of them, range and azimuth combine to locate the interface on a cross

sectional plane. The third, echo intensity, encompasses the acoustical characteristics and geometry of the reflecting interface and intervening tissue. Resolution of these three variables is severely limited by many inherent sources of error of the echo-ranging technique.

Range refers to the distance between transducer and reflecting interface. It is determined from the time interval between transmitted pulse and echo, and from an assumed value of sound velocity. Assumption of a single velocity ignores the variations found in tissue; for example, the velocity of sound is 4000 m/sec in the temporal bone, while it has a value of 1520 m/sec in the cerebral matter (26, p. 9). This particular example indicates that the selection of the velocity is a major problem when the sonic beam must travel through bone as in the examination of the brain. Among the various soft tissues there is some variance so even when there is no bone in the path, some error is still introduced.

Range resolution is theoretically limited by the width of the ultrasonic pulse. This width depends upon the shape of electric pulse that drives the transducer and on the damping characteristics of the crystal. The transducer can be represented by an underdamped second order system, so that its output, even with an ideal electrical input, will be a decaying sinusoid, which, in essence, means a longer sonic

pulse. This effect can be minimized by increasing the damping or by matching the impedance between the crystal and the coupling media (26, 31).

Azimuth, the second variable locating the reflecting interface, describes the orientation of the transducer. Resolution in azimuth is limited by the width of the transducer beam. Beam width is a function of range, and, in this consideration, the range can be divided into two general regions, the near and far field with the boundary between these two regions determined by the physical dimension of the transducer and the wave length of the sound. In the near field the beam is not divergent, and can be visualized as a cylinder. For the far field this simple model is no longer valid, and the description becomes difficult. However, the beam can be approximated by a diverging cone for which the rate of dispersion also depends upon the size of the transducer and the wave length. Some improvement can be obtained by focusing techniques similar to those used in optics. Ultrasonic lenses (26) and the parabolic reflectors (1) have been used. Regardless of the focusing technique and the degree of focusing used, there will always be a large region in which the sonic beam will have measurable width so that this will always be a limitation on the possible resolution.

Echo intensity, the amount of power transduced by the receiver, is the third variable used in diagnostic ultrasound.

Echo strength depends upon many factors; Brown (6) identifies them as follows:

1) Amount of attenuation in the path between transducer and interface
2) Angle the axis of the sound beam makes with the reflecting interface
3) Acoustical properties of the tissues forming the interface
4) Area of the interface
5) Curvature of the interface
6) Scattering properties of the interface

Obviously, it is impossible to separate any of these factors by measurements of the echo intensity only, since there are an infinite number of combinations that could produce echos with identical intensity. Even if the attenuation is taken into account by a time varying gain receiver, (signals returning shortly after the pulse is transmitted are amplified less than those returning later), and the last four factors are grouped into what may be called the reflective characteristic of the interface, it is still impossible with present techniques to isolate the effect of the angle of incidence from the reflective characteristic of the interface. Therefore, simple intensity measurements indicate nothing quantitative about the reflective characteristic of the interface which can be related to the mechanical prop-

erties of the tissue.

## Differential Diagnosis

In spite of these limitations much success has been achieved; a survey of the published work is contained in Grossman (17). As indicated by some of these reports, progress has been made in differential diagnosis, or in distinguishing similar abnormalities. Initially, the general appearance of the sonograms was the only criteria used in the diagnostic decision. This was relatively successful, since there is a striking consistency in the sonograms from different specimens with certain pathological conditions, and, in many cases, there is an equally remarkable difference in the sonograms from different abnormalities. However this general appearance is extremely sensitive to the calibration of the equipment and to the skill of the operator.

Furthermore, it is frequently misleading to attempt a diagnosis on one rather uncontrollable feature like the general appearance of the sonogram. Baum and Greenwood (3) suggest five other criteria that should be investigated in order to improve the probability of a correct diagnosis. They are:

1) Properties of the surface and interfacial area
2) Internal texture determined by spatial and intensity distributions of internal echos
3) Multiple frequency examinations

4) Enhancement techniques, for example, altering the acoustical properties of a specific structure with the temperature

5) Measurement of the energy absorbed by the tissue

By using some of these criteria many investigators have been able to distinguish relatively similar conditions with remarkable success. For example, Fujimoto et al. (14) were able to distinguish between potentially malignant thyroid neoplasms and adenomas which had already undergone cystic degeneration. They accomplished this by classifying the observed patterns with two criteria: the echos from within the lesion and the attenuation as the signal propagated through the lesion. As another example, Tanaka, et al. (37) claimed to be able to distinguish between malignant and non-malignant breast tumors. Their recognizable patterns were described as "a linear pattern, small spotted pattern, and an irregular bright pattern".

## Determination of Interface Parameters

This research effort was an attempt to evaluate a potential technique for discerning two parameters associated with the first criteria listed above, that is, the properties of the interface. The method utilizes simple power measurements to quantify both the angle of incidence and the reflective characteristic of an acoustical interface. The

goal was to develop a mathematical model that predicts the characteristics of the reflected signals. Subsequently, an attempt was made to verify this analysis by investigating several acoustical interfaces with a prototype system.

The ultimate objective of investigations in this field is to apply the technique to medical ultrasonic diagnosis. A successful system would be useful in providing additional diagnostic information when used with the simple one dimensional A-scan presentation. Furthermore, the reflective characteristic is a meaningful parameter to use for adding a gradation, or "grey" scale, to the present black and white sonograms produced by binary processing of the reflected signals.

# RELEVANT ACOUSTICAL THEORY

Before developing the multitransducer system, some relevant acoustical theory is presented, eventually leading to an expression which describes the power detected by a receiver in terms of the geometry and the properties of the transducers, and those of the reflecting interface.

## Parameters

Sound is a traveling mechanical wave whose propagation depends on the properties of the media supporting the wave and the frequency of vibration. Controlling properties of the media are density, ($kg/m^3$), and bulk modulus of elasticity, ($newtons/m^2$).

Using these two basic properties and the frequency, several other parameters can be derived. Most useful are velocity of propagation, (m/sec), wave number, (radians/m), and wave length, (m). These are related to the original properties in Equations 1, 2, and 3.

$$c = (\beta/\rho)^{1/2} \tag{1}$$

$$k = \frac{2\pi f}{c} \tag{2}$$

$$\lambda = \frac{c}{f} \tag{3}$$

where:

$c$ = velocity of sound

$\beta$ = bulk modulus of elasticity

$\rho$ = density

$f$ = frequency

$\lambda$ = wave length

## Variables

Particle velocity, (m/sec), and differential change in pressure, (newtons/$m^2$), are the most common variables used to describe a sound wave. In the remainder of this paper the word pressure implies differential change in pressure. Pressure is a scalar quantity while particle velocity is a vector quantity; both are functions of time and distance.

## Plane Waves

Plane waves, hypothetical waves characterized by planar wave fronts, are a useful concept in developing many of the basic principles of sonics, and, in certain situations they provide a good approximation to the propagation from real sources. A plane wave, or, for that matter, any type wave front, is described by its pressure and particle velocity. Expressions for a plane wave traveling in the positive x-direction are in Equations 4 and 5.

$$p = P_m \cos(\omega t - kx) \tag{4}$$

$$\bar{u} = U_{mx} \cos(\omega t - kx)\, \bar{x} \tag{5}$$

where:

$p$ = pressure

$\bar{u}$ = particle velocity

$\omega$ = angular frequency

In this discussion lower case letters are generally used to describe variables as a function of time and distance, as in Equations 4 and 5. Vector quantities will be identified by the overbar as in Equation 5. The symbol for the typical unit vector, $\bar{x}$, is also shown in this equation. The concept of phasor, (or sinor), is used in the discussion; it is symbolized by upper case letters. A phasor is a complex representation of a variable in which time has been fixed. The relationship of the phasor to the actual variable is in Equation 6.

$$p = \sqrt{2}\ \mathrm{Re}\ (P\ e^{j\omega t}) \tag{6}$$

In this equation, P is the phasor, and the "Re $(P\ e^{j\omega t})$" means the real part of the complex quantity $P\ e^{j\omega t}$. A detailed expression for P is in Equation 7;

$$P = 1/\sqrt{2}\ Pm\ e^{-jkx} \tag{7}$$

In the case of particle velocity, the phasor is a vector, like the actual variable, and this relationship is Equation 8.

$$\bar{u} = \sqrt{2}\ \mathrm{Re}\ (\bar{U}\ e^{j\omega t}) \tag{8}$$

Equation 9 defines the phasor $\overline{U}$.

$$\overline{U} = 1/\sqrt{2}\, U_{mx}\, e^{-jkx}\, \overline{x} \tag{9}$$

A more general description of the particle velocity forms Equations 10, 11, and 12.

$$\overline{u} = U_{mx} \cos(\omega t - kx)\, \overline{x} + U_{my} \cos(\omega t - ky)\, \overline{y} \tag{10}$$

$$\overline{u} = \sqrt{2}\, \mathrm{Re}\,(U_x\, e^{j\omega t})\, \overline{x} + \sqrt{2}\, \mathrm{Re}\,(U_y\, e^{j\omega t})\, \overline{y} \tag{11}$$

$$\overline{u} = |U_x|\, e^{-jkx}\, \overline{x} + |Uy|\, e^{-jky}\, \overline{y} \tag{12}$$

Mathematical expressions for variables of a wave traveling in the negative x-direction are in Equations 13 and 14. These should be compared to Equations 4 and 5 which describe the positive traveling wave.

$$p = -P_m \cos(\omega t + kx) \tag{13}$$

$$\overline{u} = U_{mx} \cos(\omega t + kx) \tag{14}$$

The phasors describing the negative traveling wave are in Equations 15 and 16. It is noteworthy that the two variables

$$P = -1/\sqrt{2}\, P_m\, e^{jkx} \tag{15}$$

$$\overline{U} = 1/\sqrt{2}\, U_{mx}\, e^{jkx}\, \overline{x} \tag{16}$$

are in phase in the case of the positive traveling wave, and $180^\circ$ out of phase for the negative traveling one.

## Acoustic Impedance

Pressure and particle velocity are interrelated, with the relationship expressed in Equation 17.

$$\bar{U} = \frac{j}{\omega\rho} \bar{\nabla} P \tag{17}$$

In this equation del, $(\bar{\nabla})$, is the standard vector operator, and $\bar{\nabla} P$ is the gradient of the pressure. Performing the operation described in Equation 17 for the positive traveling plane wave results in Equation 18.

$$U_{X+} = \frac{1}{\rho c} P_+ \tag{18}$$

Repeating this for the negative traveling wave produces Equation 19.

$$U_{X-} = -\frac{1}{\rho c} P_- \tag{19}$$

The subscripts + and - as shown in Equations 18 and 19 will be used with the phasor notation when confusion might exist.

Because of the usefulness of the relationship, it is refined by introducing specific acoustic impedance, $(m^2 sec/kg)$, which is analogous to wave impedance in electromagnetic theory. The concept implies a wave traveling in a certain direction, so it must be defined for each direction of propagation. Specific acoustic impedance of a positive traveling plane wave, a negative traveling plane wave, and a plane wave with both positive and negative traveling components are defined

in Equations 20, 21, and 22, respectively.

$$Z_{x+} = \rho c \tag{20}$$

$$Z_{x-} = -\rho c \tag{21}$$

$$Z_x = \rho c \frac{e^{-jkx} - e^{jkx}}{e^{-jkx} + e^{jkx}} \tag{22}$$

where:

$Z_{x+}$ = acoustic impedance of positive traveling wave

$Z_{x-}$ = acoustic impedance of negative traveling wave

$Z_x$ = acoustic impedance of compound wave.

## Intensity and Power

Energy of a sound wave is conveniently described in terms of sound intensity, (watts/$m^2$), which is density of power flux. It is defined in Equation 23, and, it is a vector quantity.

$$\overline{J} = \frac{\omega}{2\pi} \int_0^{2\pi/\omega} \overline{u}\, p\, dt \tag{23}$$

where:

$\overline{J}$ = sound intensity

$\omega$ = angular frequency.

For a wave in a lossless media, intensity is related to the phasor representation of the pressure and the particle velocity by Equation 24,

$$\overline{J} = P\, \overline{U}^* \tag{24}$$

where the asterisk, (*), indicates the complex conjugate of the quantity $\overline{U}$.

The acoustic power (watts) through a surface may be found by integrating Equation 25.

$$W = \iint_S \overline{J} \cdot \overline{ds} \tag{25}$$

where:

$W$ = power

$\overline{ds}$ = incremental surface vector.

## Plane Wave in a Lossy Media

To this point in the discussion energy dissipated in the media has been neglected. These losses can be accounted for by treating the wave number, k, as a complex number, that is, $k = k' - jk''$. This implies that velocity of propagation is a complex quantity, and this, in turn, produces a complex specific acoustic impedance. For positive traveling waves this complex impedance is expressed in Equation 26.

$$Z_x = | Z_x | e^{j\psi} \tag{26}$$

The phasor representation for the magnitude of particle velocity in a lossless media is in Equation 27.

$$U_x = 1/\sqrt{2}\, U_{xm}\, e^{-k''x}\, e^{-jk'x} \tag{27}$$

The phasor representation of the pressure can be determined from Equations 26 and 27; the result is Equation 28.

$$P = 1/\sqrt{2}\ P_m\ e^{-k''x}\ e^{-j(k'x - \psi)} \tag{28}$$

Time varying descriptions of the two variables are shown in Equations 29 and 30.

$$\bar{u} = U_{mx}\ e^{-k''x} \cos(\omega t - k'x)\ \bar{x} \tag{29}$$

$$p = P_m\ e^{-k''x} \cos(\omega t - k'x + \psi) \tag{30}$$

It should be noted that there is phase shift introduced by the lossy media.

The quantity $P\ \bar{U}^*$ in Equation 24 also becomes complex so that, in the general case, the sound intensity is given by the real part of this quantity as illustrated in Equation 31.

$$\bar{J} = \mathrm{Re}\ (P\ \bar{U}^*) \tag{31}$$

Reflection and Transmission of Plane Waves

Both reflection and transmission of a plane sonic wave occur at an interface or discontinuity formed by two media. Subscripts I, R, and T will be used to represent incident, reflected, and transmitted variables, respectively. The relationship between pressure and particle velocity at the interface is a boundary value problem with the following restrictions:

1) Pressure is continuous across the interface.
2) Normal component of particle velocity is continuous across the interface.
3) Angle of incidence equals angle of reflection.
4) Angle of incidence is related to angle of transmission by Equation 32.

$$\frac{\sin \gamma_I}{\sin \gamma_T} = \frac{c_I}{c_T} \tag{32}$$

Angles of incidence, reflection, and transmission are angles formed by the normal to the interface and the direction of propagation of the referenced wave.

Only two real coefficients are necessary to describe the case of normal incidence where the interface is formed by two semi-infinite, lossless media; they are the reflection coefficient and the transmission coefficient, and Equations 33 and 34 defines them.

$$R_x = \frac{|U_{xR}|}{|U_{xI}|} \tag{33}$$

$$T_x = \frac{|U_{xT}|}{|U_{xI}|} \tag{34}$$

where:

$R_x$ = reflection coefficient

$T_x$ = transmission coefficient

If the reflected and transmitted pressure and particle velocity are defined in terms of these coefficients and the incident variables, then $R_x$ and $T_x$ can be evaluated by applying the boundary conditions. This leads to the results expressed in Equations 35 and 36, where $x_o$ is the distance between the interface and the initial reference point.

$$R_x = \frac{Z_1 - Z_2}{Z_1 + Z_2} e^{-j2k_1x_o} \tag{35}$$

$$T_x = \frac{2 Z_1}{Z_1 + Z_2} e^{-j (k_1 - k_2) x_o} \tag{36}$$

In this discussion subscript 1 denotes the media supporting the incident and reflected waves, while subscript 2 refers to the region carrying the transmitted wave. If the interface is defined as the reference point, the last two equations simplify to Equations 37 and 38.

$$R_x = \frac{Z_1 - Z_2}{Z_1 + Z_2} \tag{37}$$

$$T_x = \frac{2 Z_1}{Z_1 + Z_2} \tag{38}$$

In the case of oblique incidence four parameters, or coefficients, are needed; $R_x$, which relates normal components of incident and reflected wave, $R_y$, which relates tangential components of the same waves, $T_x$ which relates normal components of incident and transmitted wave, and $T_y$ which relates

tangential components of the same waves. Defining equations for these four coefficients are analogous to Equations 33 and 34; they are in Equations 39, 40, and 41.

$$R_x = R_y = \frac{Z_1 - Z_2}{Z_1 + Z_2} \tag{39}$$

$$T_x = \frac{2 Z_1}{Z_1 + Z_2} \tag{40}$$

$$T_y = T_x \frac{C_1}{C_2} \frac{\cos \gamma_I}{[1 - (\frac{C_2}{C_1})^2 \sin^2 \gamma_I]^{1/2}} \tag{41}$$

Intensity of the reflected wave is obtained by applying Equation 31; this results in Equation 42.

$$\bar{J}_R = R_x^2 J_{xI} \bar{x} + R_y^2 J_{yI} \bar{y} \tag{42}$$

Assuming that $R_x = R_y$, leads to Equation 43.

$$\bar{J}_R = R_x^2 \bar{J}_I \tag{43}$$

For lossy media, like biological material, acoustical impedances $Z_1$ and $Z_2$ become complex, making the reflection coefficient complex. In many medical applications, the use of short sonic pulses involving the higher harmonics, further complicates the analysis, since tissue impedances are frequency dependent. Because of these considerations the reflection coefficient is an extremely complicated parameter in the case

of tissue interfaces.

If only intensity is of interest, the problem can be circumvented. Utilizing a complex reflection coefficient, variables of the reflected wave are described in Equations 44 and 45.

$$P_I = R_x P_R \tag{44}$$

$$\bar{U}_I = R_x \bar{U}_I \tag{45}$$

Intensity determined from Equation 31, is shown in Equation 46.

$$\bar{J}_R = |R_x|^2 \bar{J}_I \tag{46}$$

The phase introduced by using a complex reflection coefficient is eliminated since the conjugate of the particle velocity is involved in Equation 31.

To summarize, the amount of energy reflected depends upon the relative discontinuity of the specific acoustical impedance and upon the amount of energy incident upon the interface, or target.

## Spherical Waves

Uniform spherical waves produced by a radially pulsating sphere with a diameter much smaller than the wave length of the radiated wave are the simplest non-planar wave. Heuter and Bolt (22, p. 55) describe the pressure for this type

wave with an equation similar to Equation 47.

$$P = \frac{P_a\, e^{-jkr}}{r} \tag{47}$$

In this equation P is a constant defined by Equation 48.

$$P_a = \left[\frac{W_T \rho c}{2\pi}\right]^{1/2} \tag{48}$$

where:

$W_T$ = total radiated power

Particle velocity and pressure gradient are related by Equation 17; for the uniform spherical wave, this leads to Equation 49.

$$\overline{U} = \frac{P_a\, e^{-jkr}\, [1 + 1/(jkr)]\overline{r}}{\rho c r} \tag{49}$$

Specific acoustical impedance for the spherical wave is defined in Equation 50.

$$\overline{Z}_r = \frac{\rho c}{[1 + 1/(jkr)]} \tag{50}$$

It is noteworthy that since $k = 2\pi/\lambda$, the $1/(jkr)$ term vanishes for $r >> \lambda$ in both Equations 49 and 50 producing the simplified equations expressed in Equations 51 and 52.

$$\overline{U} = \frac{P_a\, e^{-jkr}\, \overline{r}}{\rho c r} \tag{51}$$

$$Z_r = \rho c \tag{52}$$

This last equation indicates that the specific acoustical impedance for spherical waves is approximately equal to the impedance of a plane wave.

Sound intensity of a spherical wave in a lossless media can be determined from Equation 31; the resulting expression is Equation 53.

$$\overline{J} = \frac{P_a^2 \overline{r}}{\rho c r^2} \tag{53}$$

Directed Spherical Waves

Pressure and particle velocity of sound waves produced by larger or more geometrically complicated sources can be determined by using the concept of a point source and Huyghen's principle. According to this principle any wave phenomena can be analyzed by conceptually constructing an equivalent array of point sources, and combining the effect of each elementary source. Therefore, pressure and particle velocity from any source can be determined by dividing the source into incremental elements that can be treated as point sources, and then integrating the differential pressures and particle velocities that result from the differential sources.

When this technique is applied to a circular piston, vibrating uniformly in the x, y-plane, Equation 54 results (22, p. 63).

$$P = \frac{P_r e^{-jkr}}{r} \left[ \frac{2 J_1 (ka \sin \theta)}{ka \sin \theta} \right] \tag{54}$$

where:

$a$ = radius of the source

$J_1$ = Bessel function of first kind

The constant $P_r$ is defined by Equation 55.

$$P_r = (W_T \rho c)^{1/2} \tag{55}$$

It should be noted that Equation 54 is limited to the far field because of assumptions made in the integration discussed above. This far field is the region defined by $r > \frac{4 a^2}{\lambda}$, (32, p. 6).

The bracketed term in Equation 54 is generally called the directivity function, and it relates pressure for all values of $\theta$ to the maximum value. This function is symbolized by $D_{(\theta)}$, and for the circular source described above, the directivity function is defined in Equation 56.

$$D_{(\theta)} = \frac{2 J_1 (ka \sin \theta)}{ka \sin \theta} \tag{56}$$

The expression for particle velocity of this wave is in Equation 57, which was obtained from the acoustic impedance expressed in Equation 52 and the pressure in Equation 54 with the bracketed term replaced by $D_{(\theta)}$.

$$\overline{U} = \frac{P_r e^{-jkr} D_{(\theta)} \overline{r}}{\rho c r} \tag{57}$$

Intensity of the wave can be found by applying Equation 31;

which results in Equation 58.

$$\bar{J} = \frac{P_r D^2_{(\theta)} \bar{r}}{\rho c r^2} \tag{58}$$

If the media is lossy, then the wave number, the velocity of propagation, and the acoustic impedance are treated as complex quantities as in the case of plane waves. The expression for pressure and particle velocity for non-uniform spherical waves in a lossy media are in Equations 59 and 60.

$$P = \frac{P_r e^{-k''r} e^{-j(k'r - \psi)} D_{(\theta)}}{r} \tag{59}$$

$$U_r = \frac{P_r e^{-k''r} e^{-jk'r} D_{(\theta)}}{\rho c r} \tag{60}$$

These last two equations are analogous to Equations 27 and 28 describing the plane wave.

## Reflection of Spherical Waves

Describing the reflection of spherical waves can be very difficult. The simplest case is reflection of a uniform spherical wave in a lossless media at a finite, smooth, circular, planar discontinuity perpendicular to the radius vector of the source. If the discontinuity is located in the far field and if it is relatively small, (still large in comparison with the wave length), wave fronts impinging on the interface are essentially planar. The strength of

the reflected wave depends upon the amount of energy incident on the interface and the relative values of the acoustical impedances of the two media, so total power of the reflected wave is given by Equation 61.

$$W_R = R_x^2 J S \tag{61}$$

where:

$W_R$ = reflected power

$S$ = area of the interface

The interface essentially radiates this power or acts as a source. Because of its size and geometry, it has a directivity function similar to that described in Equation 56. Pressure and particle velocity of reflected, or scattered waves produced by an interface at $r = r_o$ are in Equations 62 and 63.

$$P_R = \frac{P_r \, e^{-jk(r_o + r')} \, R_x \, S^{1/2} \, D'(\theta)}{r_o \, r'} \tag{62}$$

$$\overline{U}_R = \frac{P_R \, \overline{r}}{\rho c} \tag{63}$$

where:

$P_R$ is defined in Equation 62.

In these equations a new coordinate system with its origin at the center of the discontinuity is introduced; its variables are indicated by the prime notation.

If the interface is not perpendicular to the radius vector, the situation is analogous to oblique incidence of plane waves. Degree of obliqueness can be quantified by the angle between the radius vector drawn to the target and the normal to it; this angle is defined as the angle of incidence. Power reflected by the interface is given by Equation 64.

$$W_R = R_x^2 J_I S \cos \alpha \tag{64}$$

where:

$S$ = area of interface

$\alpha$ = angle of incidence

Pressure and particle velocity are in Equations 65 and 66; again

$$P_R = \frac{P_r e^{-jk(r_o + r')} R_x (S \cos \alpha)^{1/2} D'(\theta)}{r_o r'} \tag{65}$$

$$U_R = \frac{P_R \bar{r}}{\rho c} \tag{66}$$

where:

$P_R$ is defined in Equation 65

the primed variables refer to the origin located at the center of the interface. In the case of oblique incidence, this coordinate system is "tilted" in comparison to the one used for normal incidence, and the amount of tilt is quanti-

fied by the angle of incidence.

If the incident wave in a lossless media is non-uniform there is a directivity function associated with incident pressure and particle velocity. The power that impinges on the interface can be determined from Equation 25; however, the intensity is a function of $\Theta$ as shown in Equation 58. Therefore, the integration is extremely difficult. However, this difficulty can be circumvented if a constant intensity is assumed over the entire surface. With this assumption, the directivity function of the incident wave can be treated as a constant equal to its value at $\Theta = \Theta_o$, where $\Theta_o$ locates the position of the center of the interface with respect to the axis of the transducer. Expressions for pressure, particle velocity, and intensity are in Equations 67, 68, and 69, respectively.

$$P_R = \frac{P_r D_1(\Theta_o) e^{-jk(r_o+r')} R_x (S \cos \alpha)^{1/2} D'(\Theta')}{r_o r'} \tag{67}$$

$$\bar{U}_R = \frac{P_R \bar{r}}{\rho c} \tag{68}$$

where:

$P_R$ is defined in Equation 67

$$\bar{J}_R = \frac{P_r^2 D_1(\Theta_o) R_x^2 S \cos \alpha D'^2(\Theta') \bar{r}}{\rho c r_o^2 r'^2} \tag{69}$$

Specifying the reflected signals in a lossy media is extremely complicated because the reflection coefficient becomes complex and frequency dependent. However, intensity of the reflected signal can be determined from the intensity of the incident wave and the magnitude of the reflection coefficient, as was done for the plane wave. The result is Equation 70.

$$\bar{J}_R = \frac{P_r^2 D_1^2 (\theta_o) e^{-2k''(r_o+r_1)} |R_x|^2 S \cos \alpha D'^2(\theta')}{\rho c r_o^2 r'^2} \quad (70)$$

Reflected Power Detected by Transducer

In determining the reflected power transduced by a receiver, the principle of reciprocity is used. In simple terms, this principle states that the observed response is identical if source and measurer are interchanged. In this instance, the power observed by the receiver when treating the reflecting interface as a source is the same as the power incident on the interface if the receiver is the source. Applying this principle leads to Equation 71.

$$W_R = \frac{P_r^2 D_{1(\theta_1)}^2 D_{2(\theta_2)}^2 \cos \alpha_1 \cos \alpha_2 e^{-2k''(r_1+r_2)} R_x^2 S^2 D'^2(\theta')}{\rho c r_1^2 r_2^2} \quad (71)$$

where:

$r_1$ = distance between transmitter and reflecting interface

$r_2$ = distance between receiver and reflecting interface

$S$ = area of interface

$\alpha_1$ = angle of incidence for transmitter

$\alpha_2$ = angle of incidence for receiver

$D_1(\theta_1)$ = directivity function of transmitter

$D_2(\theta_2)$ = directivity function of receiver

$D'(\theta')$ = directivity function of interface

$R_x$ = reflection coefficient of interface

Total transmitted power is given in Equation 72.

$$W_T = \frac{P_r^2}{\rho c} \tag{72}$$

where:

$W_T$ = total transmitted power

Substituting this last relationship into Equation 71 results in Equation 73.

$$W_R = \frac{W_r D_1^2(\theta_1) D_2^2(\theta_2) \cos \alpha_1 \cos \alpha_2 e^{-2k''(r_1+r_2)} R_x S D'^2(\theta')}{r_1^2 r_2^2} \tag{73}$$

Grouping the last three terms in Equation 73 into a single constant called the reflection characteristic of the interface eliminates the problems of defining size, shape, con-

cavity, and scattering properties of the interface. Equation 74 defines this constant. Substituting this into Equation 73 yields an expression

$$R = R_X \, S \, D'_{(\theta')} \tag{74}$$

where:

$R$ = reflection characteristic

$R_X$ = reflection coefficient (defined in Equation 37)

describing received power as a function of transmitted power, transducer characteristics, interface location, and reflective characteristic. The result is Equation 75.

$$W_R = \frac{W_T \, D_{1(\theta_1)}^2 \, D_{2(\theta_2)}^2 \cos \alpha_1 \cos \alpha_2 \, e^{-2k'(r_1+r_2)} \, R^2}{r_1^2 \, r_2^2} \tag{75}$$

This equation will be used to develop analytical expression for the reflected powers in the multitransducer system described in the next chapter.

# SYSTEM ANALYSIS

Before developing the mathematical model for the various multitransducer configurations investigated, it is necessary to define the interface parameters and to specify the measured variables.

The parameter used to describe the interface is the reflection characteristic introduced in Equation 74. This parameter is represented by the symbol R, and it includes the reflection coefficient defined in Equation 37, the scattering properties of the interface, and other undefined terms.

To quantify this reflection characteristic, it is necessary to introduce two other interface parameters. Angle of incidence of the sonic beam on the interface, represented by the symbol $\alpha$, is defined as the angle between the normal to the interface and the axis of the transmitting transducer. Range, symbolized by r, is the distance from transmitting crystal to the interface along its normal.

Reflection time, defined as the time between transmitted and received pulses, is one of the measured variables; it is represented by T. The other measured variables are the peak voltages of the returning signals; these will be represented by $V_1$ and so on, corresponding to the individual receivers.

Mathematical Analysis of Two Transducer System

Relationship between desired parameters and measurable variables are obtained by applying Equations 75 and 76. The latter is introduced here.

$$2r = Tc \tag{76}$$

where:

$r$ = range

$T$ = reflection time

It results from the fact that in the echo time T, a pulse propagating at a constant velocity c will travel from the transducers to the target and back, a distance of 2r.

Figure 1 shows a schematic representation of the two-transducer system. Transducer #1 functions as a transmitter and receiver, while #2 serves only as a receiver. Radial distance to the interface along its normal is represented by r, $\alpha$ is the angle of incidence, $\beta$ describes the orientation of the second transducer with respect to the first, and $\delta$ indicates the separation between the centers of the two transducer faces.

In determining the expression for the transduced powers, it is assumed that all radial distances are equal to r, which is justified since only the power is of interest. Also, since $r >> \delta$, the angle $\gamma$ was approximated by $\delta/r$. With these assumptions, application of Equation 75 to the receiver yields

Equations 77 and 78.

$$W_1 = \frac{K_1 W_T D_{1(\alpha)}^4 \cos^2 \alpha R^2 e^{-4k''r}}{r^4} \quad (77)$$

$$W_2 = \frac{K_2 W_T D_1^2 (\alpha-\delta/2r) D_2^2 (\alpha+\delta/2r-\beta) \cos^2 \alpha R^2 e^{-4k''r}}{r^4} \quad (78)$$

where:

$W_1$ = power of receiver #1

$W_2$ = power of receiver #2

Many of the terms in these last two equations can be combined by introducing the notation $A_1$, which is defined in Equation 79.

$$A_1 = \frac{K W_T e^{-4k''r}}{r^4} \quad (79)$$

Also, since the transducers are considered to be identical in acoustical characteristics, the constants $K_1$ and $K_2$ can be replaced by a single constant, and $D_{(\theta)}$ can be substituted for $D_{1(\theta)}$ and $D_{2(\theta)}$. The $\cos^2 \alpha$ term can be eliminated because $|\alpha| < 3^\circ$, and for this range $\cos^2 \alpha \approx 1$. These simplifications lead to Equations 80 and 81.

$$W_1 = A_1 R^2 D^4_{(\alpha)} \quad (80)$$

$$W_2 = A_1 R^2 D^2_{(\alpha-\delta/2r)} D^2_{(\alpha+\delta/2r-\beta)} \quad (81)$$

Because the peak values of the voltages representing the returning echos are proportional to the square-root of the transduced power, an expression for these voltages can be obtained by taking the positive square root of the right-hand side of Equations 80 and 81. This yields Equations 82 and 83, where A includes the proportionality constant.

$$V_1 = A\,R\,D^2_{(\alpha)} \tag{82}$$

$$V_2 = A\,R\,|D_{(\alpha-\delta/2r)}|\;|D_{(\alpha+\delta/2r-\beta)}| \tag{83}$$

In the latter equation, the absolute value signs on the directivity functions are necessary to assure the positive square root. By taking the ratio, these two equations can be combined resulting in Equation 84.

$$\frac{V_1}{V_2} = \frac{D^2_{(\alpha)}}{|D_{(\alpha-\delta/2r)}|\;|D_{(\alpha+\delta/2r-\beta)}|} \tag{84}$$

and Equation 82 can be solved for R producing Equation 85.

$$R = \frac{V_1}{A\,D^2_{(\alpha)}} \tag{85}$$

Interface parameter r which appears in these equations can be determined from Equation 74 and measurement of the reflection time T. However, if the variation in range is limited to a narrow, specified region, then it can be treated

as a constant. This means that $\delta/2r$ and A can also be considered constant. With this consideration, Equations 84 and 85 now involve only known constants, measurable variables, and the two unknown target parameters. These two equations can now be solved simultaneously for the two interface parameters.

However, an analytical solution is not possible because of the Bessel function contained in the directivity function $D_{(\theta)}$, but the solution can be obtained by a numerical or graphical technique. A graph of $V_1/V_2$ versus $\alpha$ can be constructed by numerical computation so that for a measured value of $V_1/V_2$, the angle of incidence $\alpha$ can be determined. Once $\alpha$ is known, Equation 85 can be used to evaluate the reflection characteristic R. In determining this parameter, a graphical technique must again be used to find $D^2_{(\alpha)}$ which appears in Equation 85.

Feasibility of various transducer arrangements was investigated by constructing the graph of $V_1/V_2$ versus $\alpha$ from Equation 84. This was done primarily to see if there was a unique relationship between $\alpha$ and $V_1/V_2$; in other words, to test if $\alpha$ is a single-valued function of $V_1/V_2$. Uniqueness is necessary in order to prevent any ambiquity in determining $\alpha$ from measured values of $V_1$ and $V_2$.

The first configuration examined consisted of two parallel transducers with a 11/16 inch spacing between centers.

With this arrangement, $\beta = 0$ and $\delta = 11/16$ inch. A value of $r = 9$ inch was used so that $\delta/2r = 2^{\circ}$, and ka, the parameter in the directivity function, was set equal to 50. The resulting curve is shown in Figure 2. An examination of this figure indicates that the relationship is not unique, and, therefore, this arrangement is unacceptable. An example will illustrate this problem; for $V_1/V_2 = 5$, $\alpha$ could be $\pm 1.8^{\circ}$ or $\pm 2.8^{\circ}$.

Two parallel transducers with a wider separation, ($\delta = 2$ inch), was also investigated; all other constants were the same. The result is shown in Figure 2, and the conclusion is the same as above.

The final two-transducer system was a non-parallel configuration with $\beta = 2^{\circ}$, $\delta = 11/16$ inch, and all other constants the same. The resulting curve is also shown in Figure 2; again the problem of uniqueness exists. Because of these repeated failures it was concluded that a two-transducer system was inadequate, so, a third receiver was added.

## Mathematical Analysis of Three Transducer System

A schematic diagram of the three transducer system is shown in Figure 3. The center crystal serves as a transmitter and receiver, while the other two are receivers.

The equation describing the measured voltages for receiver #1 and #2 are identical to those for the two-

transducer system, and they are given in Equations 82 and 83. For the third receiver, the expression is analogous to Equation 83, and is in Equation 86.

$$V_3 = A\,R\,|D_{(\alpha+\delta/2r)}|\;|D_{(\alpha-\delta/2r+\beta)}| \tag{86}$$

This last equation can be combined with Equation 82 to produce Equation 87, which is similar to Equation 84.

$$\frac{V_1}{V_3} = \frac{D^2(\alpha)}{|D_{(\alpha+\delta/2r)}|\;|D_{(\alpha-\delta/2r+\beta)}|} \tag{87}$$

A numerical analysis similar to those performed on the two-transducer systems was performed using Equations 84 and 87. The resulting curves for $\beta = 2^\circ$, and $\delta = 11/16$ inch, are shown in Figure 4. An examination of this figure indicates that a unique value of $\alpha$ can be found for experimentally determined values of $V_1/V_2$ and $V_1/V_3$. For example, a value of $V_1/V_2 = 4$ implies that $\alpha = 1.6^\circ$ or $\alpha = -3^\circ$; however if $V_1/V_3 = 0.4$ is also given, then $\alpha$ must be $-3^\circ$. Once $\alpha$ is known, the reflection characteristic, R can be determined from Equation 85. Therefore, this analysis indicates that measurements of the reflected intensity by the three-transducers system can be used to quantify the angle of incidence, $\alpha$, and the reflection characteristic, R, provided assumption made in developing the mathematical model are valid in the real problem.

# EXPERIMENTAL RESULTS

To verify the analysis in the previous chapter and to determine some of the limitations and practical problems associated with this technique, a simple prototype system was constructed. Since only known interfaces were examined in this evaluation, it was not necessary to actually use the third transducer in the evaluation procedure.

## System Description

Two identical transducers[1] with resonant frequencies of 2 MC are rigidly mounted in a plastic fixture with $\beta = 2^{o}$, (as described in Figure 1). To allow angular motion of the entire fixture with a minimal variation in transducer location, this assembly is supported by a rod at the top and springs at the bottom as shown in Figure 5. The upper rod is attached to a linear micromanipulator, and, since the transducer assembly is free to pivot on it, the angular orientation of the transducer can be controlled and quantified by the manipulator's vernier.

Other system components are: a pulsing circuit, receiver amplifier and detectors, and an oscilloscope.[2]

---

[1] Model G-Z-7-2.250, Metrix, Inc., 11122 East 47th St., Denver, Colorado.

[2] Type 564 with 3A1 vertical channel amplifier, Tektronix, Inc., Beaverton, Oregon.

A block diagram is shown in Figure 6.

The pulsing circuit excites Transducer #1 producing a short ultrasonic pulse which is directed toward the target. Some of the energy is reflected by the target and received by all transducers. These signals are amplified, rectified, and integrated to produce a voltage pulse whose peak value is proportional to the received intensity. The oscilloscope displays the voltage pulse, and its peak value is determined visually. Resulting values correspond to the voltages described by Equations 82 and 83.

## Electronic Circuits

A circuit diagram of the pulsing circuit and the receiver amplifiers is shown in Figure 7. The pulsing circuit consists of a R-C capacitor discharge circuit to produce a short high voltage pulse with extremely fast rise time (300 nanosec.). The capacitor, initially changed from a high voltage source, is instantaneously connected directly to the transducer using a SCR switch. A fast pulse so generated shock excites the ceramic piezoelectric transducer crystal causing it to oscillate at its natural mechanical frequency, and a damped sine wave train results.

Because it is difficult to construct a fast acting switch that will alternately connect pulser and receiving amplifier to the transducer, the receiver and pulser are connected directly in parallel. An input clipping circuit

in the receiver input limits the magnitude of the exciting pulse to a level that will not adversely effect the receiver.

The receiver amplifiers are formed primarily by linear integrated circuits.[1] Individual gain control is obtained by the 5 K Ω variable resistors and the 500 K Ω variable resistor functions as a dual sensitivity control. The output is rectified by the detector diode, the input impedance of the oscilloscope provides the proper time constant for the integration.

## Calibration

In the development of the system model, it was necessary to make two assumptions about the hardware that require validation. The first is that the sonic axis of the transducers are related by the angle as shown in Figure 1. Careful construction which insured that the physical axes were properly oriented was not sufficient since discrepancies between physical and sonic axes of a transducer are possible (42). Therefore, after construction of the transducer assembly, the orientation of each crystal was tested to determine if adjustments were required. The location of the sonic axes were established by operating each transducer as a transceiver and adjusting the manipulator's vernier for maximum reflection. The vernier scale on the manipulator was

---

[1]Type CA 3022, Radio Corporation of America, Electronic Components and Devices, Harrison, New Jersey.

used to quantify and compare the orientation of the axes. For the transducers used in this work the two axes coincided so no adjustments were needed.

Similarity of the receivers was the second assumption about the hardware. This implies, first of all, that the transducers were equally efficient, or equally damped. To verify this, each transducer was adjusted for normal incidence and operated as a transceiver. A comparison of the reflected signals displayed on the oscilloscope indicated that the transducers used had similar damping characteristics. The second implication of this assumption was that the amplifiers had equal sensitivities. A calibration procedure insured that this was true.

## Verification of Analysis

Because of the assumptions and simplifications made in the theoretical analysis leading to Equations 84, 85, and 87, verification is proper. To determine the validity, $V_1$ and $V_2$ were measured for various values of $\alpha$ with a known interface. These measured values were plotted and an attempt was made to match the data with analytical curves determined from Equations 82 and 83 by varying the system constants ka, $\delta/2r$, and $\beta$. This variational approach is appropriate since the analytical curves are extremely sensitive to the value used for these constants and their true values cannot be determined accurately without much more sophisticated equip-

ment.

Voltage measurements were made as $\alpha$ was varied in $1/4^{\circ}$ steps between $\pm 3.5^{\circ}$ in both directions, that is, for increasing and decreasing values of $\alpha$. The small angular variations were obtained by adjusting the micromanipulator. The vernier scale was used to quantify the angle since the linear and angular displacement are related by a sinusoidal function. By repeating the process, four sets of data were obtained. A hysteresis effect in the mechanical adjusting fixture produced an offset between the data obtained for increasing and decreasing values of $\alpha$. To compensate for this, the data sets collected for increasing values of $\alpha$ were shifted forward $1/8^{\circ}$; while the sets for decreasing values of $\alpha$ were moved back the same amount.

The test interface was formed by immersing an acrylic plastic block,[1] (4 inch x 5 inch x 1 inch), in a water bath. This discontinuity approximates the flat, smooth, semi-infinite, perfect reflector, for which the reflection characteristic is identical to the reflection coefficient defined in Equation 37. An expression for the acoustical impedance found in this last equation is given in Equation 52. Constants used in determining the R for this water-acrylic plastic interface were found in Weast (40, p. E37),

---

[1] Plexiglas®, Cadillac Plastic and Chemical Co., 15111 Second Ave., Detroit, Michigan.

and they are listed below:

| Acrylic plastic | Water |
|---|---|
| $\rho$ = 1.18 gr/cc | $\rho$ = 1.00 gr/cc |
| c = 2680 m/sec | c = 1540 m/sec |

Performing the calculation produces a value of R = 0.34.

Figure 8 is a plot of the measured values of $V_1$ versus the angular setting of the mechanical adjusting fixture, referred to as the control $\alpha$ and identified by $\alpha_c$. Superimposed on this data are curves representing Equation 82 for ka equal to 60, 65, and 70. The value of A was determined by solving Equation 82 for A, and substituting the measured value of $V_1$ with $\alpha$ = 0 and the value of R listed above, (R = 0.34); the directivity function with $\alpha$ = 0 is equal to unity. An examination of Figure 8 indicates that Equation 82 with ka equal to 60 or 65 matches the data reasonably well.

Experimental values of $V_2$ along with curves representing Equation 83 are plotted as a function of $\alpha c$ in Figures 9 and 10. The latter shows curves for ka equal to 60, 65, and 70 with $\beta = \delta/2r = 2^\circ$; while the former contains curves for ka = 65 with the following combination of values for $\delta/2r$ and $\beta$:

$$\delta/2r = 2^\circ, \ \beta = 2^\circ$$
$$\delta/2r = 1.5^\circ, \ \beta = 1.5^\circ$$
$$\delta/2r = 2^\circ, \ \beta = 2.5^\circ$$

For $V_2$ the match between the analytical curves and the experimental data is not as good as it was for $V_1$. The curves with $\delta/2r = \beta = 2°$ and ka equal 60 or 65 provide the best match for $V_2$.

In summary, the mathematical model developed in the analysis produces results that agree reasonably well with experimental data with small discrepancies near the extremes of the curves. Mismatch in those regions probably is a result of errors introduced by assuming intensity is constant over the aperture of the receiver which has a solid angle of about 2°. This assumption, made in the analysis just prior to Equation 67, implies that the integral of curves similar to those shown in Figures 8, 9, and 10 over a 2° range can be approximated by a constant which is proportional to its value at the center of the range. Because of the shape of these curves, this approximation would be inaccurate near the extremes.

## Determination of Constants

Before evaluating the technique with other interfaces, values must be selected for the constants, ka, $\delta/2r$, and $\beta$. To optimize this selection, the effect of these constants in calculating R's and $\alpha$'s were investigated. From the measured voltages for the water-acrylic plastic interface, $\alpha$'s and R's were computed using Equations 84 and 85 with several combinations of constants. Values of $\alpha$ and R

determined in this way will be referred to as experimental $\alpha$ and experimental R and identified by $\alpha_e$ and $R_e$; the angular setting of the mechanical adjusting fixture will be identified as the control $\alpha$ and represented by $\alpha_c$; and the value of R determined above from Equation 37 will be called the theoretical R and symbolized by $R_T$.

Figures 11, 12, 13, and 14 contain the results of this study. The first is a plot of $\alpha_e$ versus $\alpha_c$ with $\delta/2r = \beta = 2^\circ$ and ka equal to 60, 65, and 70; the ideal relationship is also shown. Figure 12 is a similar plot with ka fixed at 65 and the following combinations for the other two constants:

$$\delta/2r = 2^\circ, \ \beta = 2^\circ$$
$$\delta/2r = 1.5^\circ, \ \beta = 1.5^\circ$$
$$\delta/2r = 2^\circ, \ \beta = 2.5^\circ$$

The third of these drawings contains curves of $R_e$ as a function of $\alpha_c$ for $\delta/2r = \beta = 2^\circ$ and ka equal to 60 and 65. Figure 14 indicates the effect of $\delta/2r$ and $\beta$ on $R_e$; curves with $ka = 65$ and the combinations of $\delta/2r$ and $\beta$ listed above are shown. A horizontal line representing the theortical value of R, $(R = 0.34)$, is also included in these last two drawings.

An examination of these four figures, particularly Figure 13, indicates that the combination of $\delta/2r = 2^\circ$ and $\beta = 2^\circ$ provides a closer match to the ideal situation. The

preferred value of the third constant, ka, is not so obvious; both ka = 60, and ka = 65 seem equally acceptable. Therefore, in computing the R's and $\alpha$'s for the other interfaces examined, two combinations of constants were used; they are:

$$ka = 60,\ \beta = 2^{o},\ \delta/2r = 2^{o}$$
$$ka = 65,\ \beta = 2^{o},\ \delta/2r = 2^{o}$$

## Examination of Other Interfaces

To evaluate the extensibility of the technique to other interfaces and to discover some of its limitations, two other interfaces were investigated. Voltage measurements were made of the reflected signals from interfaces formed by water and aluminum and by water and polyethylene.[1] The procedure was identical to that described previously, including the compensation for mechanical hysteresis. Using Equations 84 and 85, experimental R's and $\alpha$'s were computed from this data for the two sets of constants listed at the end of the previous section.

Figures 15, (ka = 60), and 16, (ka = 65), show the experimental $\alpha$'s determined for various values of $\alpha_c$. Ideally, the measured value would be identical to the control value, so the theoretical relationship is a straight-line

---

[1]Epolene® C-10, Eastman Chemical Products, Inc., Kingsport, Tennessee.

represented by $\alpha_e = \alpha_c$, and this is shown on Figures 15 and 16. For comparison purposes, dashed lines represent a linear approximation of the experimental data. An examination of these two curves indicates that a value of ka = 65 produces a closer correlation between the experimental data and the ideal relationship for both interfaces. Further, the lines representing the water-aluminum interface for both values of ka are closer to the ideal relationship than the curves of the other interface. Since the measured voltages differ greatly for these two interfaces, (2.2 v to 0.13 v for normal incidence), a non-linearity in the data processing would account for this discrepancy. The abrupt discontinuities in experimental data occurring when $\alpha_c$ is about $-1.75^\circ$ and $1^\circ$, coincide with the minimum and maximum of the $V_2$ curve shown in Figure 21. The error introduced by the integration assumption discussed in connection with the attempt to match $V_2$ data with an analytical expression, is probably the principle component of the distortion.

Experimental R's for the water-aluminum and water-polyethylene interface with ka equal to 60 and 65 are shown in Figures 17 and 18, respectively. The horizontal lines indicate the values of $R_T$; they were calculated by assuming an ideal interface and using Equations 39 and 52. Values for density and velocity for the various media are listed in Weast (40, p. E37); they are:

| Water | Aluminum | Polyethylene |
|---|---|---|
| $\rho$ = 1.00 gr/cc | $\rho$ = 2.7 gr/cc | $\rho$ = 0.90 gr/cc |
| c = 1540 m/sec | c = 6420 m/sec | c = 1950 m/sec |

The resulting value for the water-aluminum interface is $R_T$ = 0.84, and the value for the water-polyethylene interface is $R_T$ = 0.064.

For $\alpha$ between $\pm$ 1° the experimental values agree fairly well with the theoretical one, but outside this range there is little correlation between $R_e$ and $R_T$. This lack of correlation probably is the product of the abrupt discontinuities in the data describing $\alpha_e$ (See Figures 15 and 16), since its value is used in determining R. Dispersion of the data can be accounted for by relatively small computational inaccuracies, ("round-off" errors), and experimental errors, (tolerance on $\alpha_c$ was about 0.1° and on the voltage measurements about 5%). Since the directivity function has such a steep slope, (see Figure 8), any error in determining $\alpha$ is amplified considerably in calculating R.

# CONCLUSIONS

This technique offers a simple method, utilizing relatively standard equipment, for determining the reflective characteristic of acoustical interfaces. Accuracy demonstrated for limited values of $\alpha$ with the prototype system was about 10 to 15% for R and about $0.5^{\circ}$ for $\alpha$. The major source of error was the inadequacy of the mathematical model for certain regions of $\alpha$. Improvements in the model should increase the accuracy and extend the applicable region to values of $\alpha$ between $\pm 3.5^{\circ}$. With this increase in accuracy, the technique would most probably be useful in medical ultrasonic diagnosis and should certainly be pursued.

In future work refinements of the mathematical model should be investigated. The model might be improved by using a different set of values for constants A, ka, $\delta/2r$, and $\beta$. A curve matching technique to reduce the discrepancy between the analytical curves and the experiment data might be developed to optimize the selection of these constants. Certainly, the model would be enhanced by a better approximation for the integral of the intensity over the aperture of the receiver than its center value. This refinement would reduce the error in determining R for regions of $\alpha$ corresponding to the extremes of the directivity function. A possible approach would be to divide the aperture into smaller segments, and assign weighting factors to each

segment. The average value of the intensity for each segment and its weighting factor could be used to approximate the integral of the intensity.

Another possibility is experimentally establishing a set of calibration or standard curves. These curves would essentially be a graphical representation of the relationship between $\alpha$ and the voltage ratio and between $AD^2_{(\alpha)}$ and $\alpha$, and they would be utilized to evaluate $\alpha$ and R from the measured voltage. Data obtained from several types of interfaces, perhaps even biological ones, should be processed to produce these standard curves.

In any experimental work done in the future, certain hardware improvements would be desirable. An angular manipulator would result in more accurate setting for the control $\alpha$ than the linear one used in this work. A peak detector circuit would be helpful in measuring the peak value of $V_1$ and $V_2$, and a digital readout would improve the consistency of these measurements. A range gating process would eliminate a potential problem of extraneous reflection.

In the prototype system, both transceiver and receiver were narrow-beam transducers. The possibility of using a broad-beam device for either transceiver, receiver, or both should be examined.

# BIBLIOGRAPHY


1. Asberg, A. Ultrasonic cinematography of the living human heart. Ultrasonics 5:113-117. 1967.

2. Baum, G. Instrumentation problems in ophthalmic ultrasonography. Ultrasonics 6:43-47. 1968.

3. Baum, Gilbert and Greenwood, Ivan A. Current status of ophthalmic ultrasonography. In Kelly, Elizabeth. Ultrasonic energy. Pp. 260-277. Urbana, Illinois, University of Illinois Press. 1965.

4. Berkowitz, Raymond S., ed. Modern radar analysis, evaluation, and system design. New York, New York, John Wiley and Son, Inc. c1965.

5. British Association for the Advancement of Science. Mathematical tables. Vol. 6. Cambridge, England, University Press. 1937.

6. Brown, T. G. Visualization of soft tissue in two and three dimensions - limitations and developments. Ultrasonics 5:118-124. 1967.

7. Damascelli, B., Cascinelli, N., Livraghi, T., and Veronesi, U. Preoperative approach to thyroid tumors by a two-dimensional pulsed echo technique. Ultrasonics 6:242-243. 1968.

8. Donald, I. and Brown, T. G. Demonstration of tissue interfaces within the body by ultrasonic echo sounding. British Journal of Radiology 34:539-545. 1961.

9. Edler, Inge. Mitral valve function studied by the ultrasound echo method. In Grossman, C. C., Holmes, J. H., Joyner, C. R., and Purnell, E. W., eds. Diagnostic ultrasound. Pp. 198-228. New York, New York, Plenum Press. 1966.

10. El Piner, Isaak Efimovich. Ultrasound physical, chemical, and biological effects. New York, New York, Consultant Bureau. 1964.

11. Fleming, J. E. E. and Hall, A. J. Two dimensional compound scanning-effects of maladjustments and calibration. Ultrasonics 6:160-166. 1968.

12. Frederick, Julian R. Ultrasonic engineering. New York, New York, John Wiley and Son, Inc. c1965.

13. Friedlander, F. G. Sound pulses. Cambridge, England, University Press. 1958.

14. Fujimoto, Y., Oka, A., Omoto, R., and Hirose, M. Ultrasound scanning of the thyroid gland as a new diagnostic approach. Ultrasonics 5:177-180. 1967.

15. Garg, A. G. and Taylor, A. R. An investigation into the effect of pulsed ultrasound on the brain. Ultrasonics 5:208-212. 1967.

16. Grossman, C. C. Acoustic phenomena in ultrasonic detection of brain tumor. Ultrasonics 3:22-24. 1965.

17. Grossman, C. C., Holmes, J. H., Joyner, C. R., and Purnell, E. W., eds. Diagnostic ultrasound. New York, New York, Plenum Press. 1966.

18. Herrey, Erna M. J. Approximation formula for the radiation resistance of a piston set in an infinite wall. Journal of the Acoustical Society of America 25: 154-155. 1963.

19. Holmes, J. H. The present status of ultrasonic diagnostic techniques in internal medicine. Ultrasonics 5:60-66. 1967.

20. Holmes, Joseph H. Ultrasonic diagnosis of liver disease. In Grossman, C. C., Holmes, J. H., Joyner, C. R., and Purnell, E. W., eds. Diagnostic ultrasound. Pp. 249-263. New York, New York, Plenum Press. 1966.

21. Holmes, Joseph H. Ultrasonic studies of the bladder and kidney. In Grossman, C. C., Holmes, J. H., Joyner, C. R., and Purnell, E. W., eds. Diagnostic ultrasound. Pp. 465-480. New York, New York, Plenum Press. 1966.

22. Hueter, Theodore F. and Bolt, Richard H. Sonics. New York, New York, John Wiley and Son, Inc. c1955.

23. Joyner, C. R. Reflected ultrasound in the diagnosis of tricuspid stenosis. American Journal of Cardiology 19:66-73. 1967.

24. Kelly, Elizabeth, ed. Ultrasonic energy, biological investigations and medical applications. Urbana, Ill., University of Illinois Press. 1965.

25. Kelly, Elizabeth, ed. Ultrasound in biology and medicine. Washington, D.C., American Institute of Biological Sciences. 1957.

26. Kossoff, G., Robinson, D. E., and Garrett, W. J. The C.A.L. abdominal echoscope. C.A.L. (Commonwealth Acoustical Laboratory, Department of Health), Miller's Point, Sydney, Australia Report No. 31. 1965.

27. Kossoff, G., Robinson, D. E., and Garrett, W. J. Two dimensional ultrasonography in obstetrics. In Grossman, C. C., Holmes, J. H., Joyner, C. R., and Purnell, E. W., eds. Diagnostic ultrasound. Pp. 333-347. New York, New York, Plenum Press. 1966.

28. Lehman, J. Stauffer, Evans, George C., and Brady, Luther W. Ultrasound exploration of the spleen. In Grossman, C. C., Holmes, J. H., Joyner, C. R., and Purnell, E. W., eds. Diagnostic ultrasound. Pp. 264-295. New York, New York, Plenum Press. 1966.

29. Lufkin, E. G., Alfrey, A. C., Trucksess, M., and Holmes, J. H. Early diagnosis of polycystic kidney disease. Clinical Research 14:382. 1966.

30. Makow, D. M. and Real, R. R. Immersion ultrasonic brain examination - 360° compound scanning. Ultrasonics 3: 75-80. 1965.

31. McShimin, H. J. Performance of high frequency barium titanate transducers for generating ultrasonic waves in liquids. The Journal of the Acoustical Society of America 31:1519-1522. 1959.

32. Micsky, L. I. von. Ultrasonic tomography in obstetrics and gynecology. In Grossman, C. C., Holmes, J. H., Joyner, C. R., and Purnell, E. W., eds. Diagnostic ultrasound. Pp. 348-368. New York, New York, Plenum Press. 1966.

33. Morse, Philip M. and Ingard, K. Uno. Theoretical acoustics. New York, New York, McGraw-Hill Book Co., Inc. c1968.

34. Purnell, E. W. Ultrasound in ophthalmological diagnosis. In Grossman, C. C., Holmes, J. H., Joyner, C. R., and Purnell, E. W., eds. Diagnostic ultrasound. Pp. 95-110. New York, New York, Plenum Press. 1966.

35. Randall, Robert H. An introduction to acoustics. Cambridge, Mass., Addison-Wesley Press, Inc. 1951.

36. Reid, John M. A review of some basic limitations in ultrasonic diagnosis. In Grossman, C. C., Holmes, J. H., Joyner, C. R., and Purnell, E. W., eds. Diagnostic ultrasound. Pp. 1-12. New York, New York, Plenum Press. 1966.

37. Tanaka, Wagai, T., Kikuchi, Y., Uchida, R., and Uematsu, S. Ultrasonic diagnosis in Japan. In Grossman, C. C., Holmes, J. H., Joyner, C. R., and Purnell, E. W. Diagnostic ultrasound. Pp. 27-45. New York, New York, Plenum Press. 1966.

38. Tarnoczy, T. Sound focusing lenses and wave guides. Ultrasonics 3:115-127. 1965.

39. Vlieger, M. de. Evolution of echo-encephalography in neurology - a review. Ultrasonics 5: 91-97. 1967.

40. Weast, Robert C. CRC handbook of chemistry and physics, 48th ed. Cleveland, Ohio, The Chemical Rubber Co. 1967.

41. Wells, P. N. T. and Evans, K. T. An immersion scanner for two dimensional ultrasonic examination of the human breast. Ultrasonics 6:220-228. 1968.

42. White, D. Naldrett. The limitation of echo-encephalography. Ultrasonics 5:88-90. 1967.

43. Wolff, Irving and Malter, Louis. Directional radiation of sound. Journal of the Acoustical Society of America 2:201-241. 1930.

ACKNOWLEDGEMENTS

I wish to thank all of the people who have assisted and advised me. I particularly want to express my appreciation to Dr. Neal Cholvin and Dr. David Carlson, my co-major professors, for their cooperation, guidance, and encouragement throughout all phases of my graduate program. Dr. Carlson also served as research advisor, and his suggestions and assistance made this project possible.

# APPENDIX

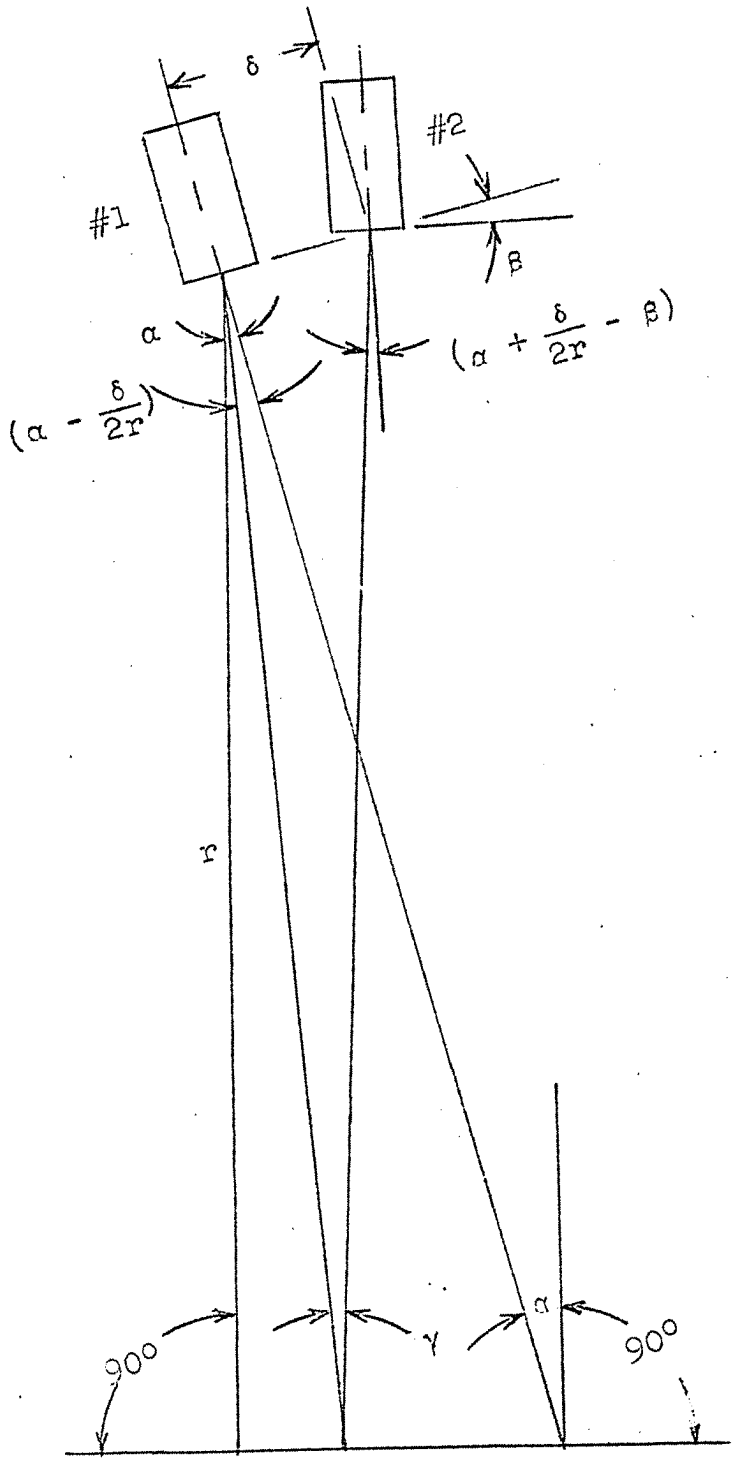


Figure 1. Schematic diagram of two transducer system

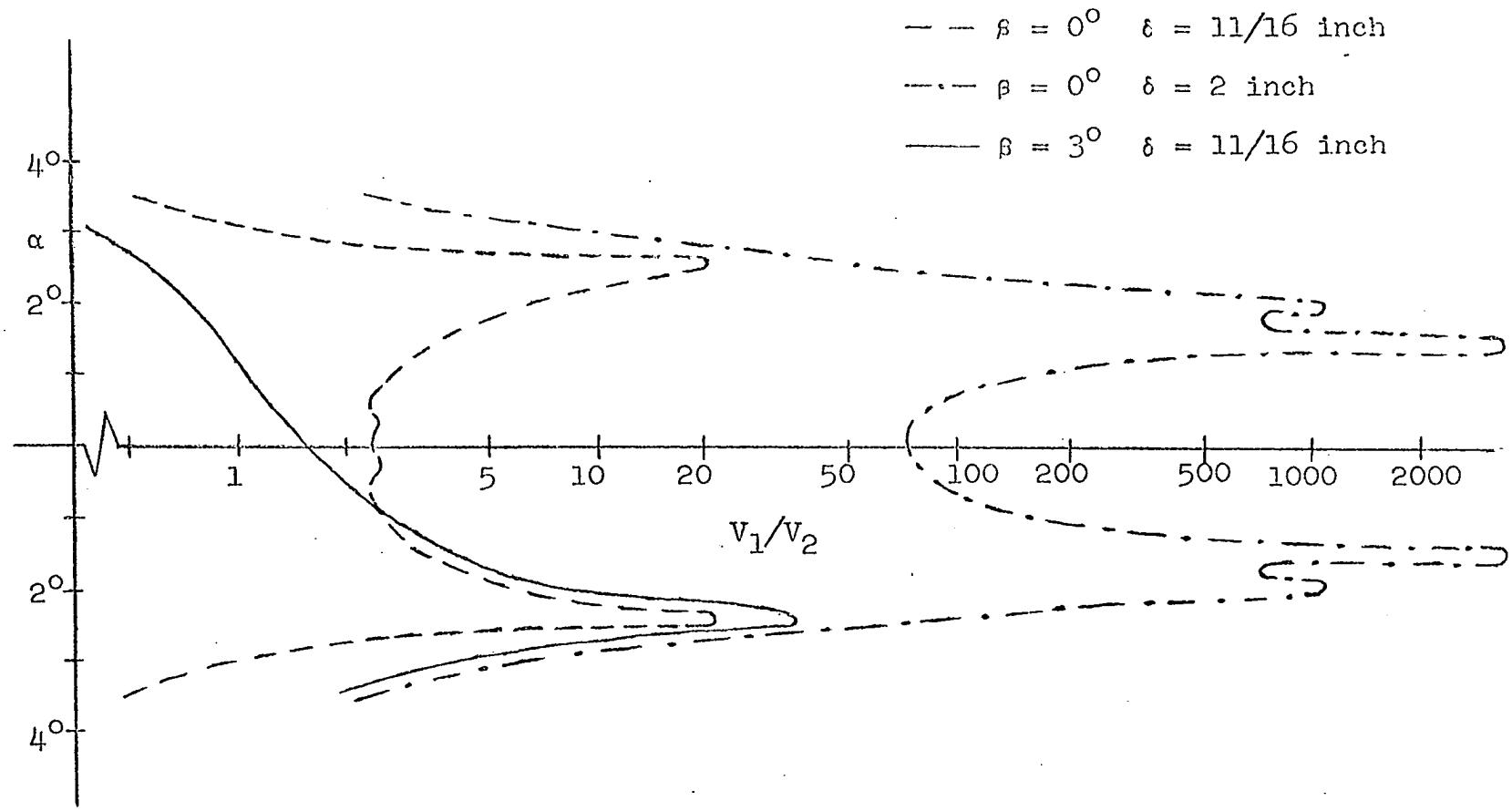


Figure 2. Graph showing analytical curves of α as a function of $V_1/V_2$ for various two transducer configurations

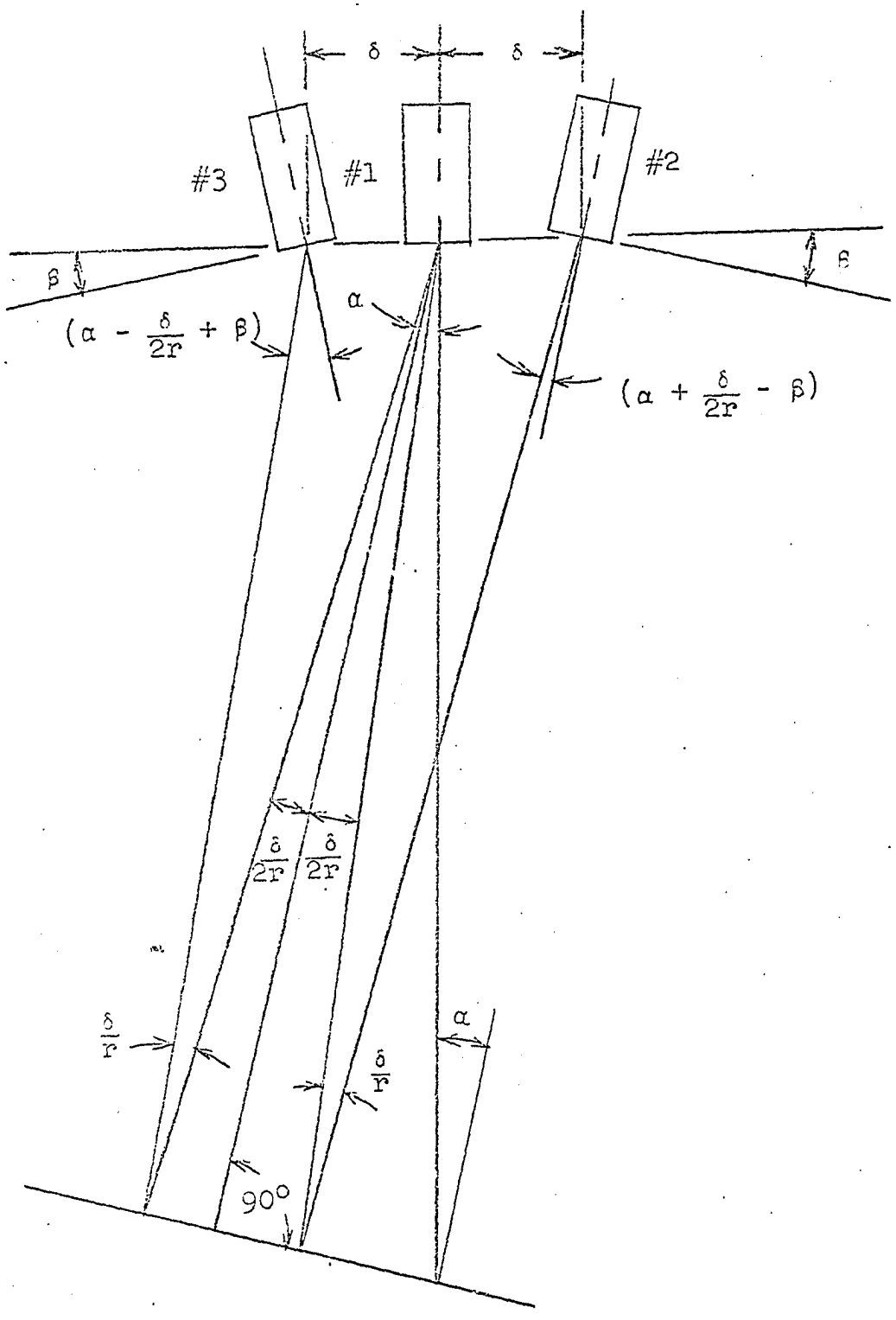


Figure 3. Schematic diagram of three transducer system

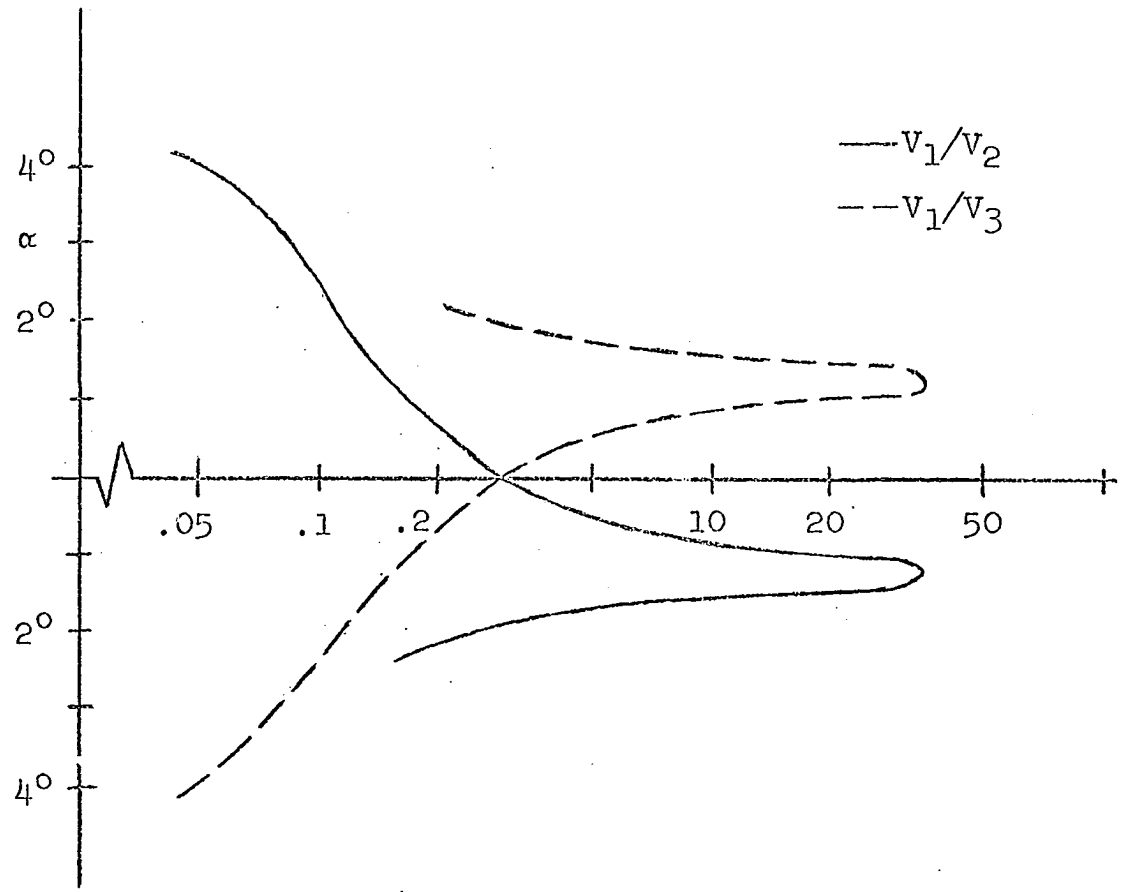


Figure 4. Graph showing analytical curves of α versus $V_1/V_2$ and $V_1/V_3$ for three transducer system

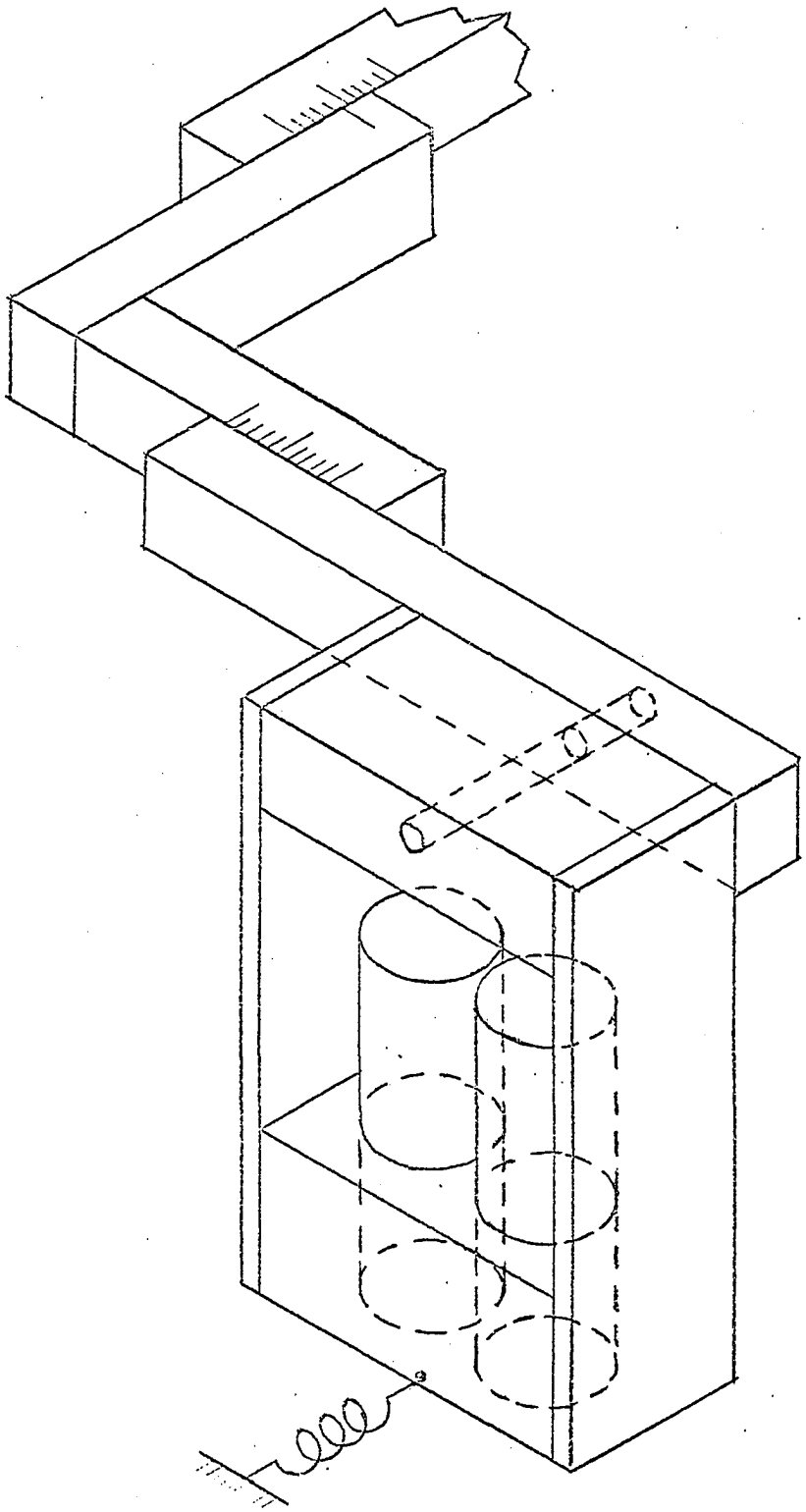

Figure 5. Angular adjusting fixture

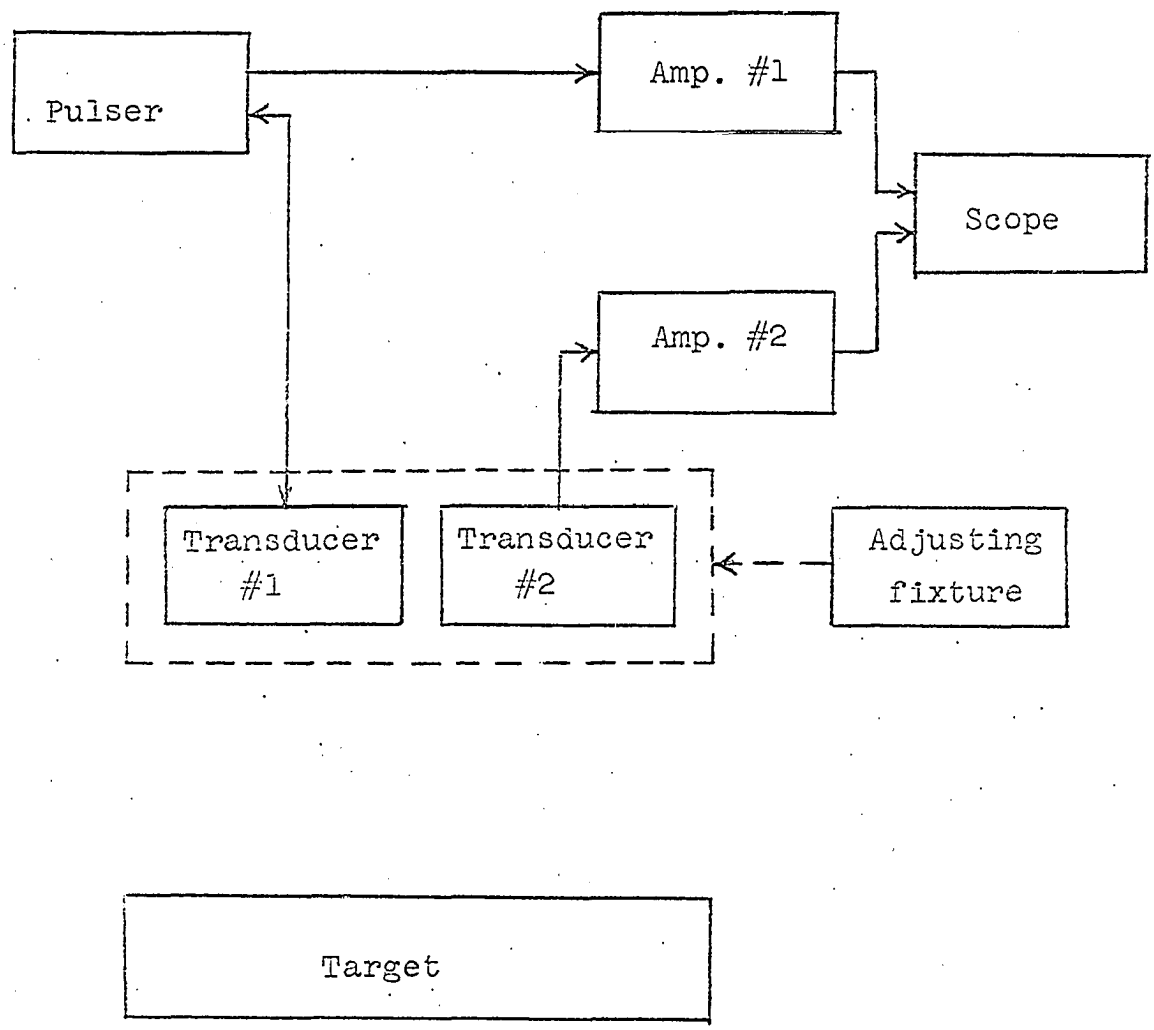


Figure 6. Block diagram of system

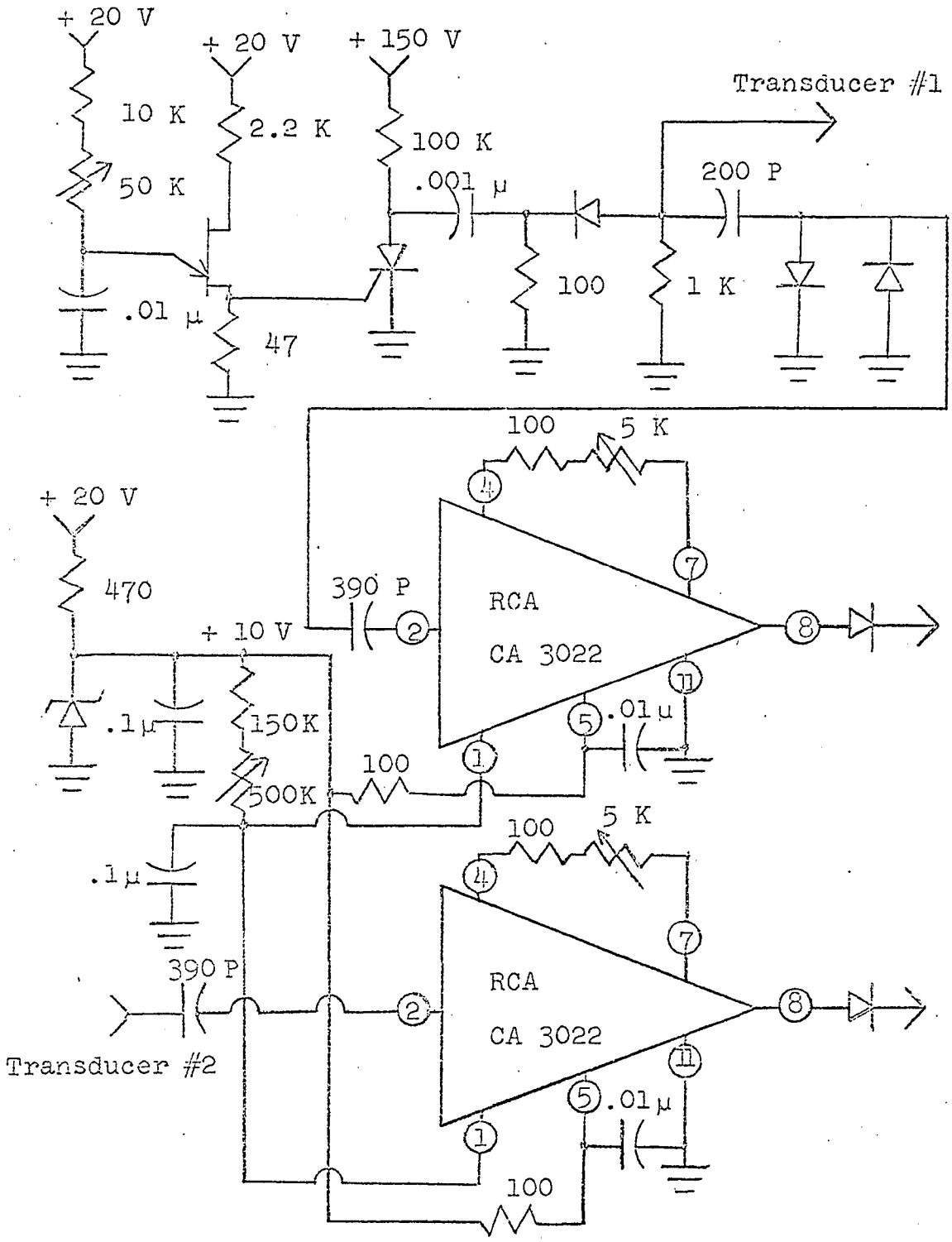


Figure 7. Circuit diagram of pulsing circuit and receiver amplifiers

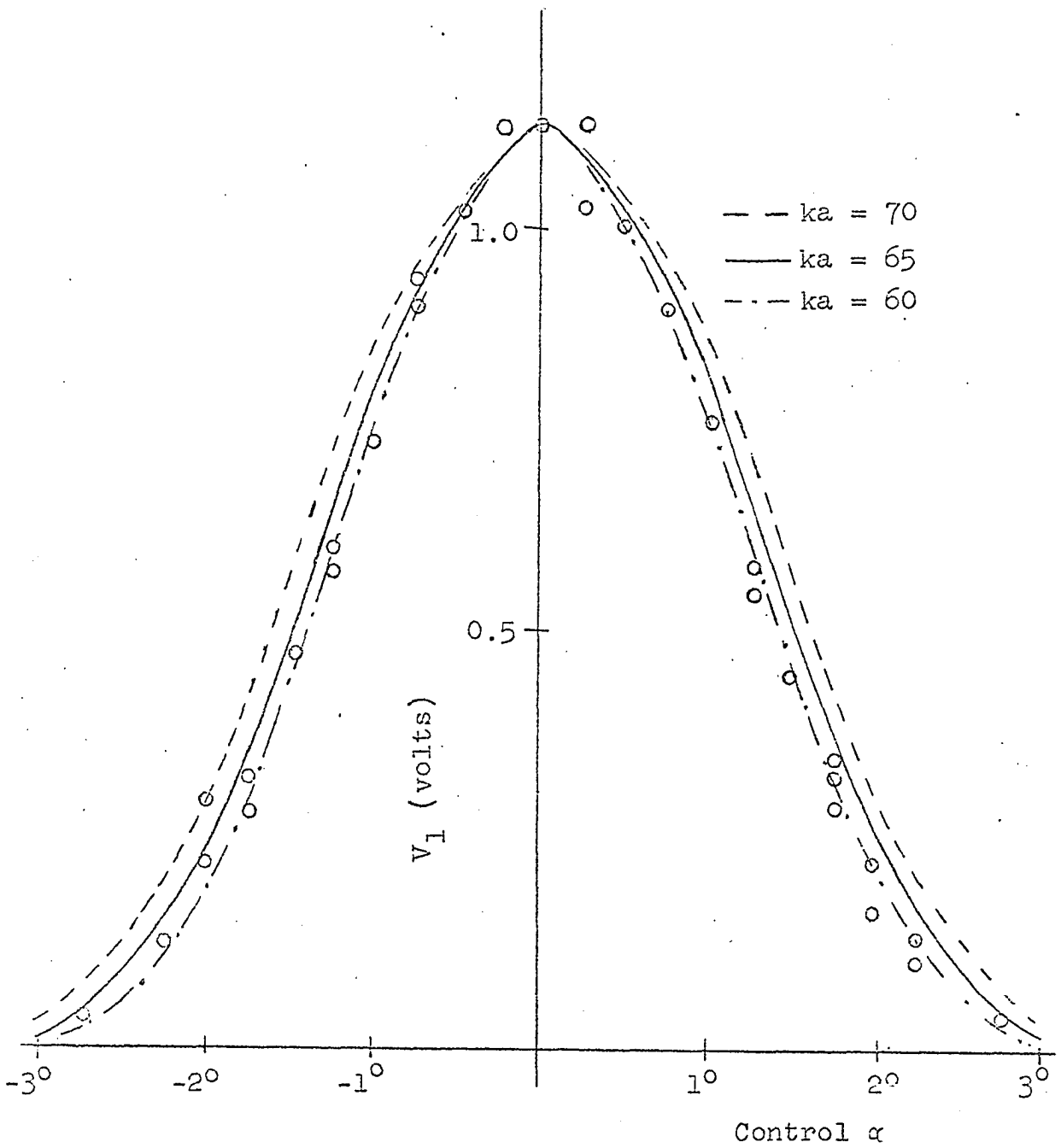


Figure 8. Graph showing the experimental values of $V_1$ and curves representing the analytical expression for $V_1$ evaluated with $\beta = \delta/2r = 2^\circ$ and various ka. The reflecting surface was a water-acrylic plastic interface.

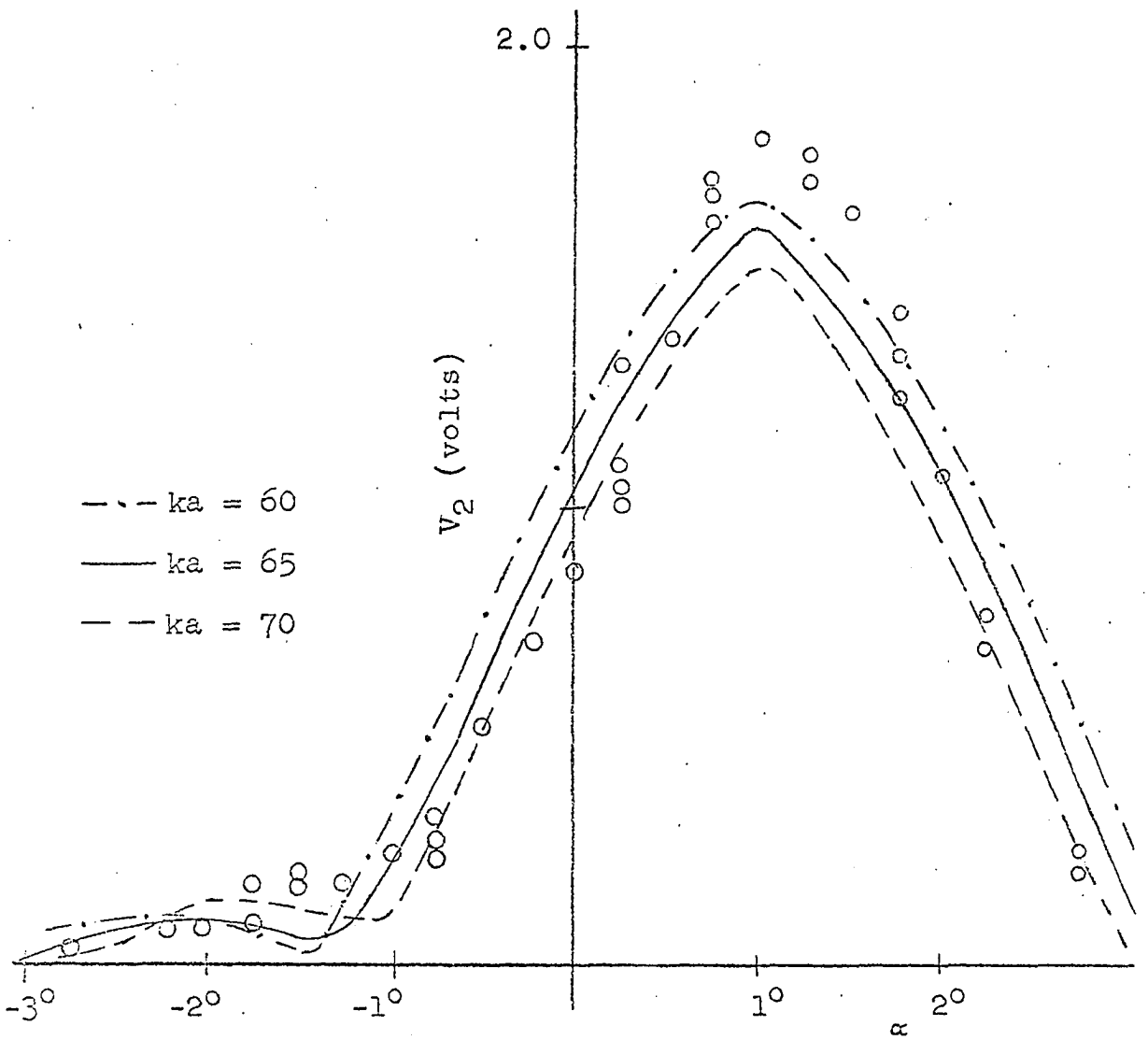


Figure 9. Graph showing the experimental values of $V_2$ and curves representing the analytical expression for $V_2$ evaluated with $\beta = \delta/2r = 2^\circ$ and various ka. The reflecting surface was a water-acrylic plastic interface.

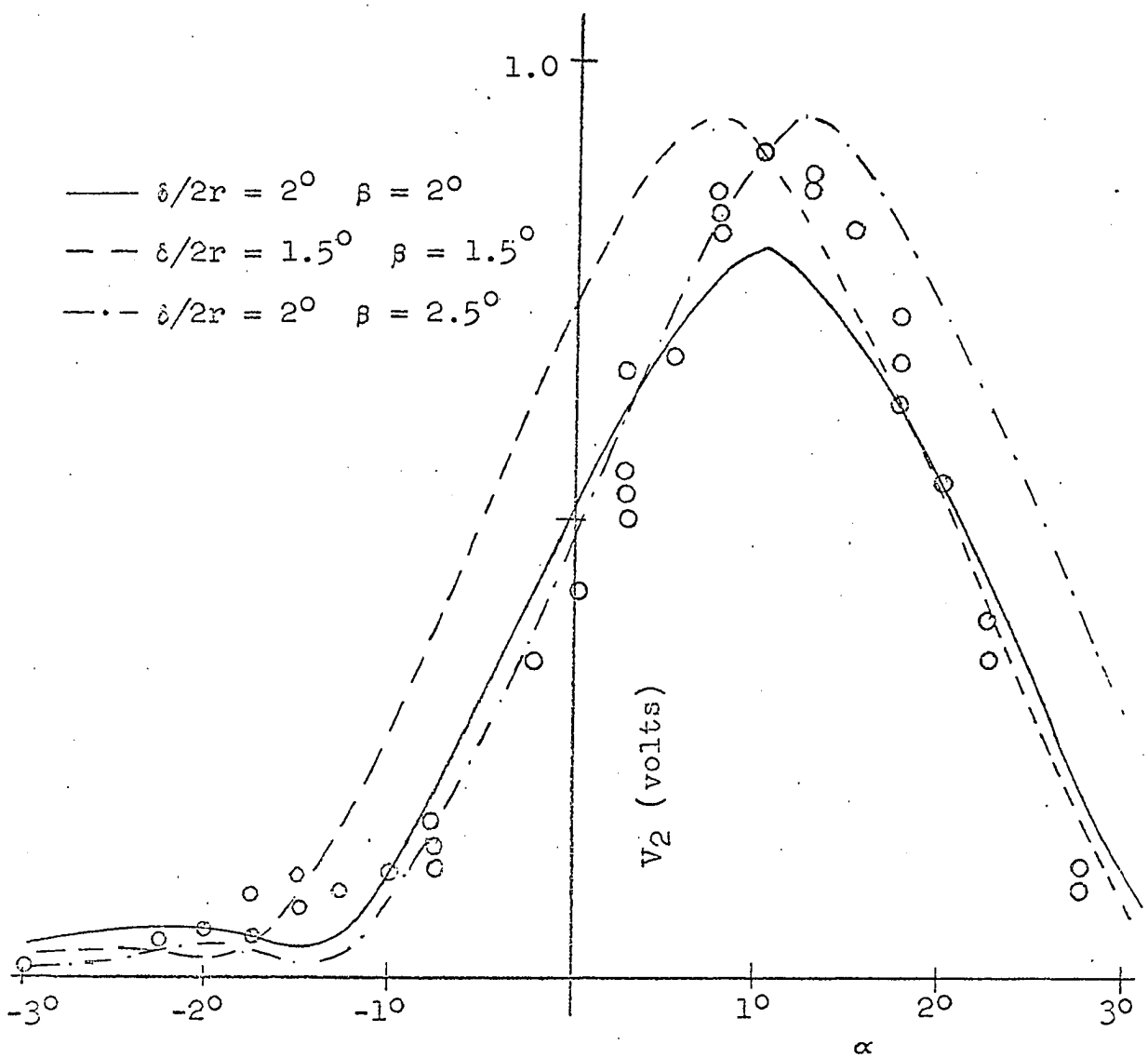


Figure 10. Graph showing the experimental values of $V_2$ and curves representing the analytical expression for $V_2$ evaluated with ka = 65 and various β and δ/2r. The reflecting surface was a water-acrylic plastic interface.

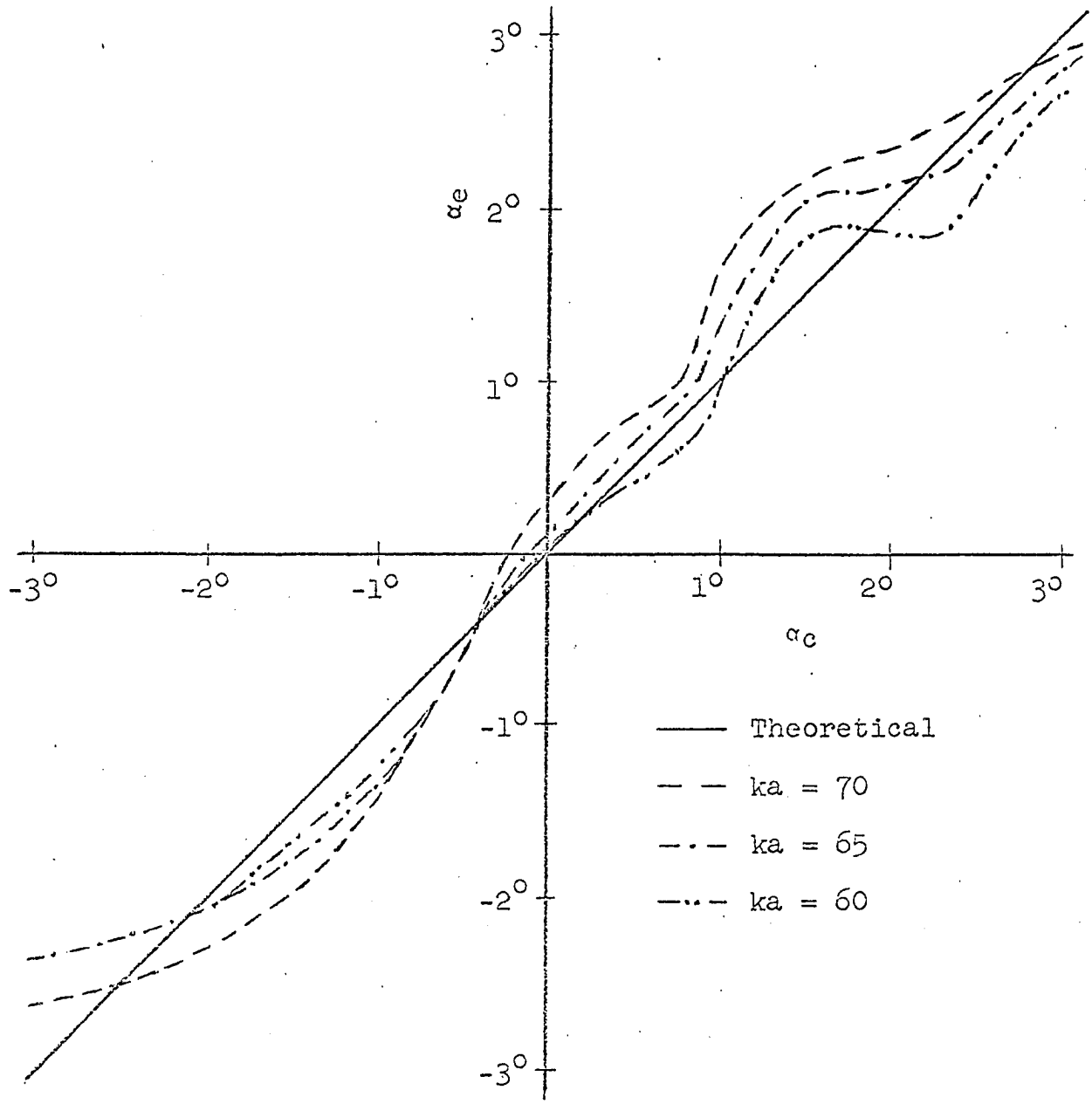


Figure 11. Graph showing the theoretical and experimental relationship between $\alpha_e$ and $\alpha_c$ with $\beta = \delta/2r = 2^\circ$ and various ka. The reflecting surface was a water-acrylic plastic interface.

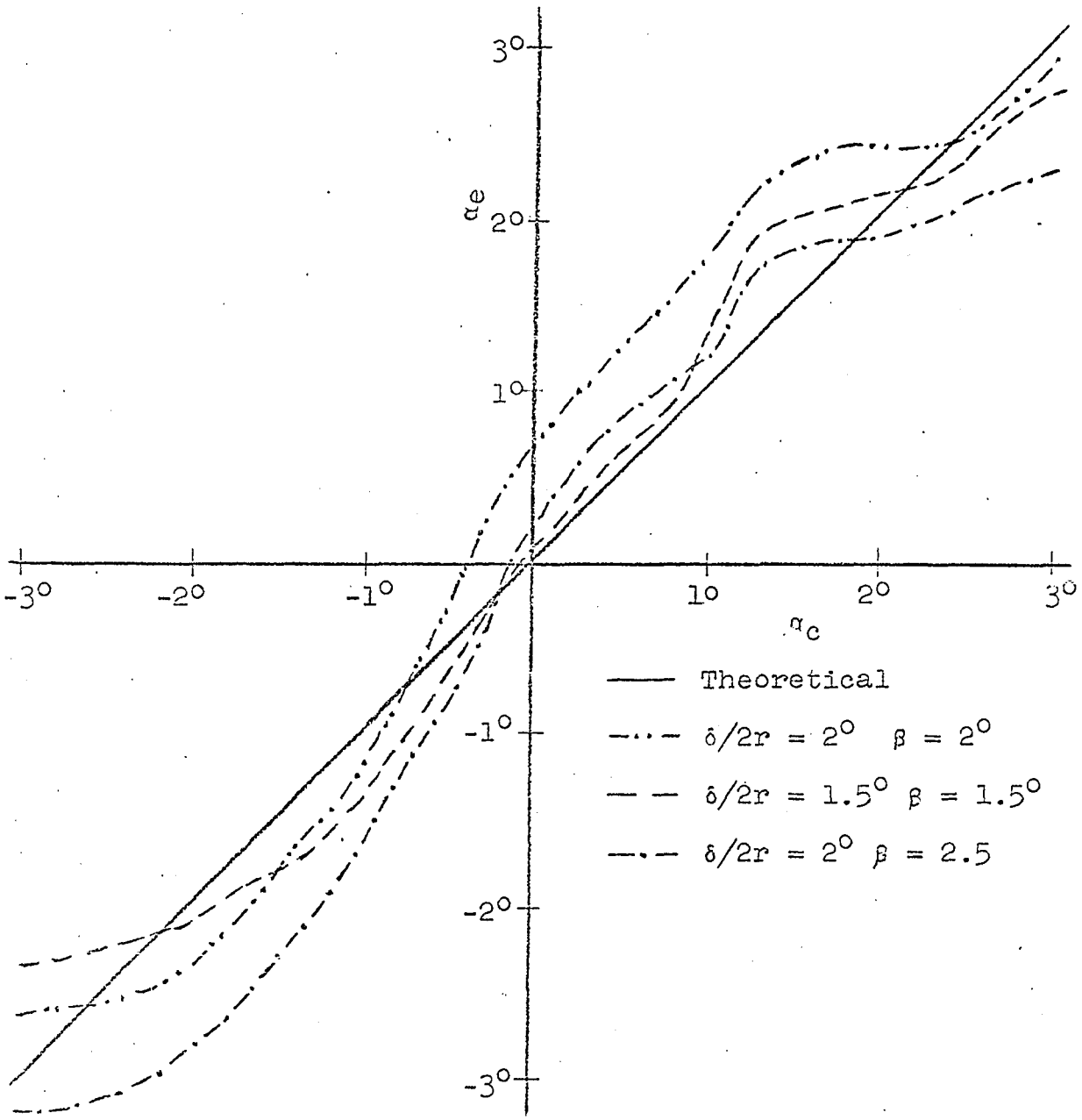


Figure 12. Graph showing the theoretical and experimental relationship between $\alpha_e$ and $\alpha_c$ with ka = 65 and various β and δ/2r. The reflecting surface was a water-acrylic plastic interface.

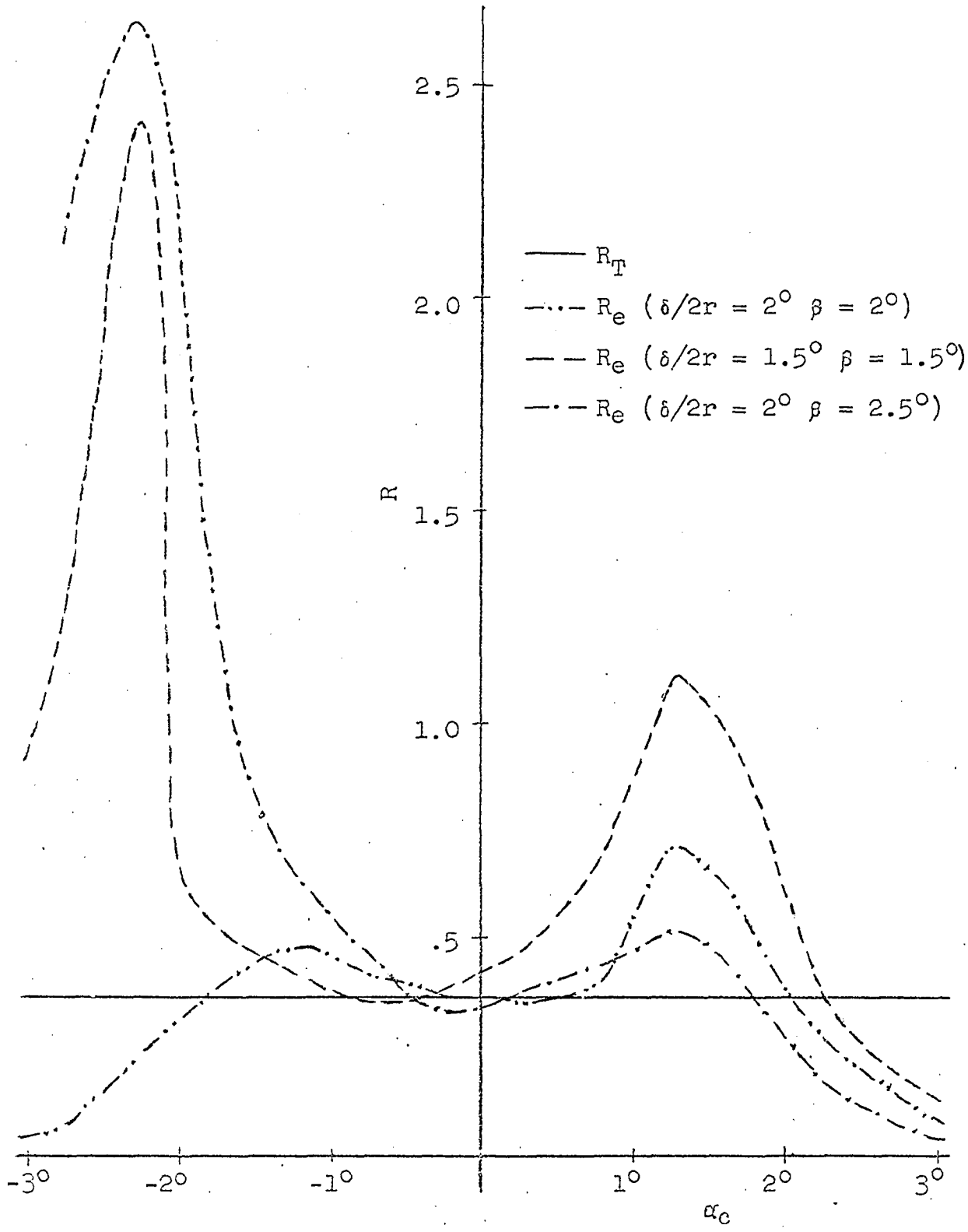


Figure 13. Graph showing $R_T$ and $R_e$ evaluated with ka = 65 and various $\beta$ and $\delta/2r$. The reflecting surface was a water-acrylic plastic interface.

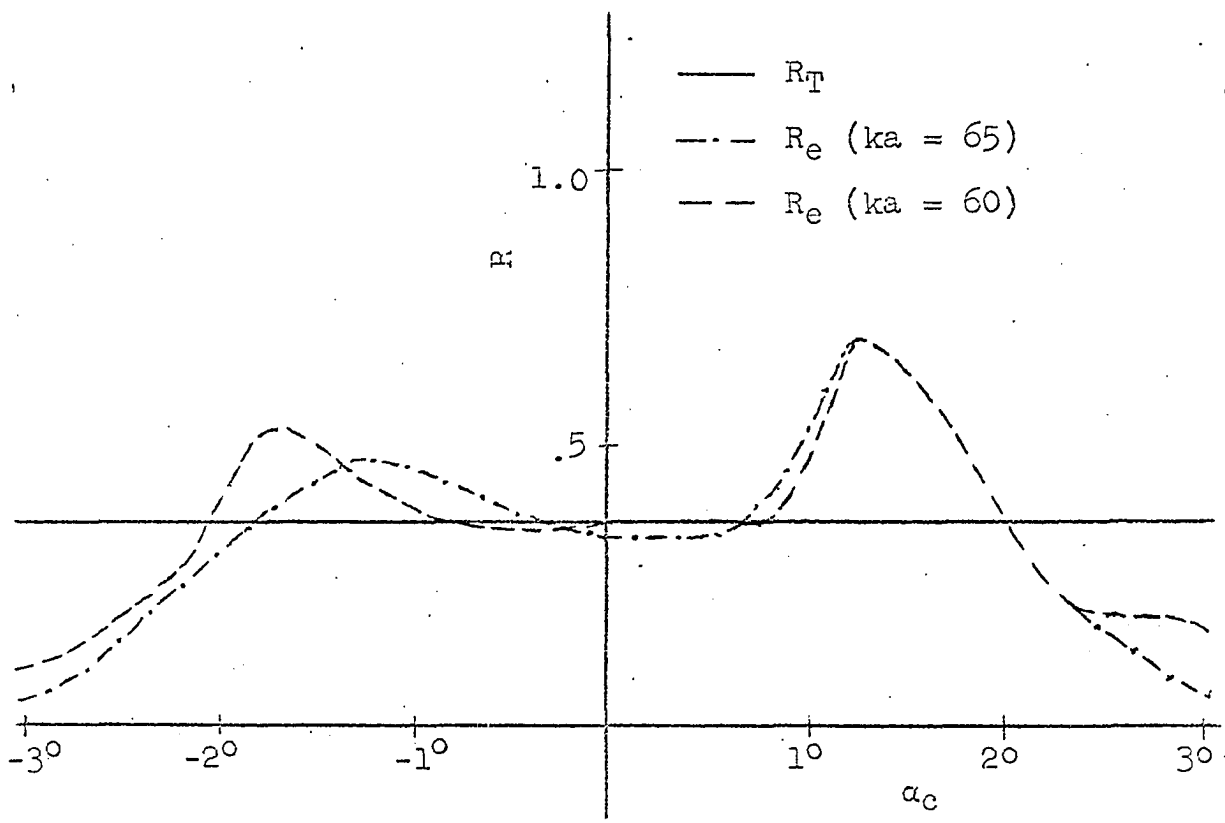


Figure 14. Graph showing $R_T$ and $R_e$ evaluated with $\beta = \delta/2r = 2^o$ and various ka. The reflecting surface was a water-acrylic plastic interface.

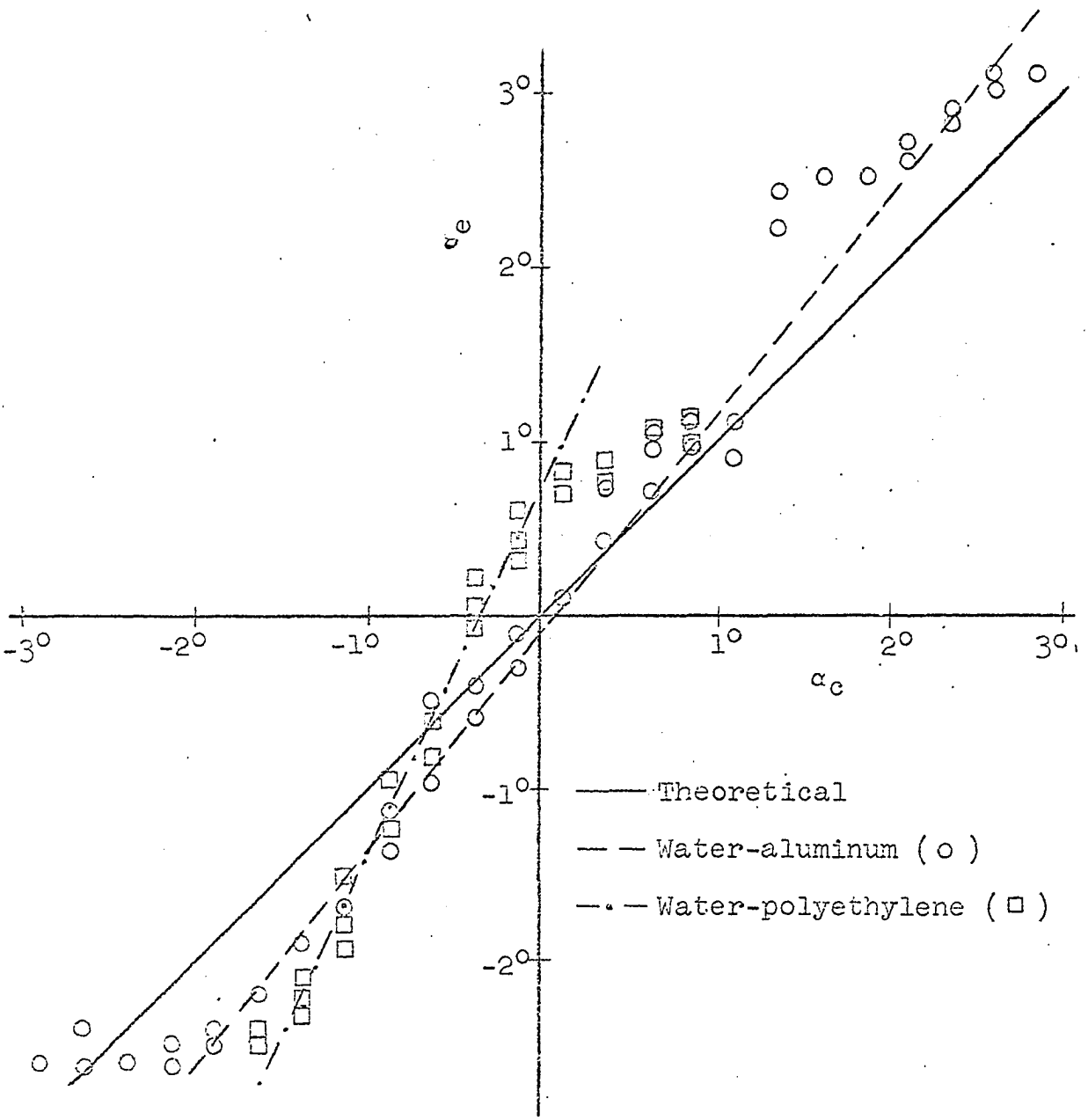


Figure 15. Graph showing the theoretical relationship between $\alpha_e$ and $\alpha_c$, experimental values of $\alpha_e$, (evaluated with ka = 60, $\beta = \delta/2r = 2^\circ$), and straight-line approximations to the data.

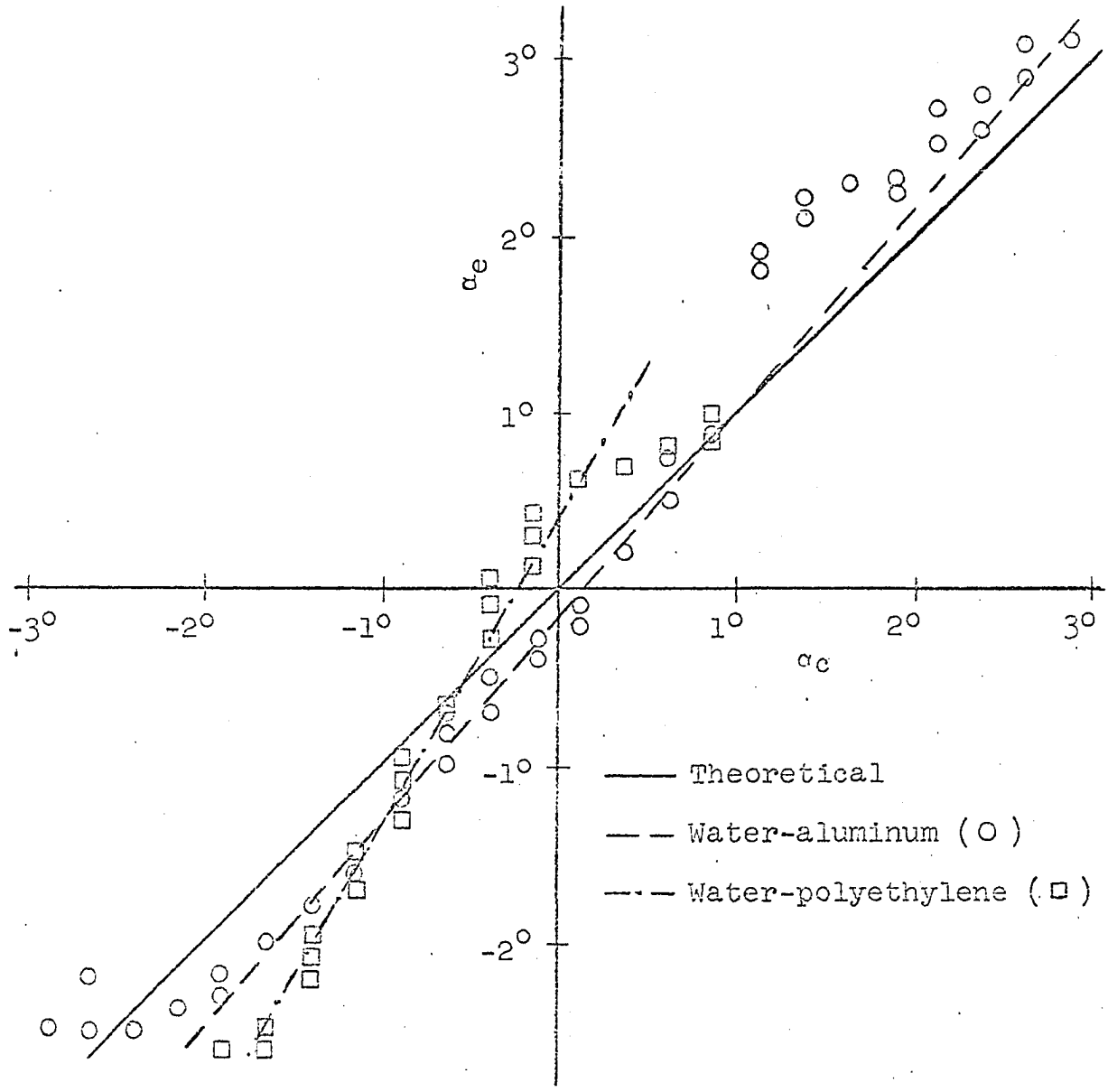


Figure 16. Graph showing the theoretical relationship between $\alpha_e$ and $\alpha_c$, experimental values of $\alpha_e$, (evaluated with $ka = 65$, $\beta = \delta/2r = 2^\circ$), and straight-line approximations to the data.

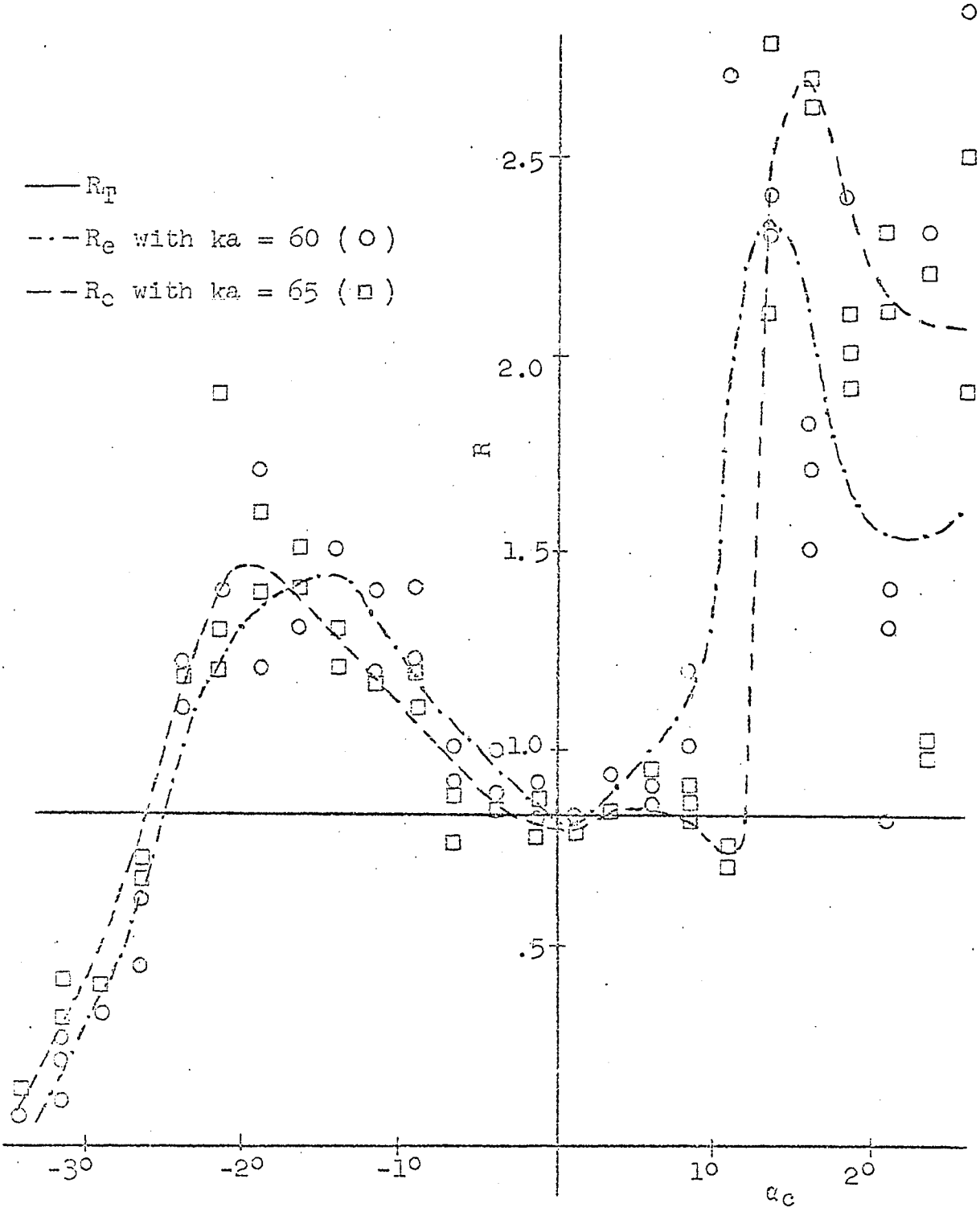


Figure 17. Graph showing $R_T$ and $R_e$ evaluated with $\beta = \delta/2r = 2^\circ$ and various ka. The reflecting surface was a water-aluminum interface.

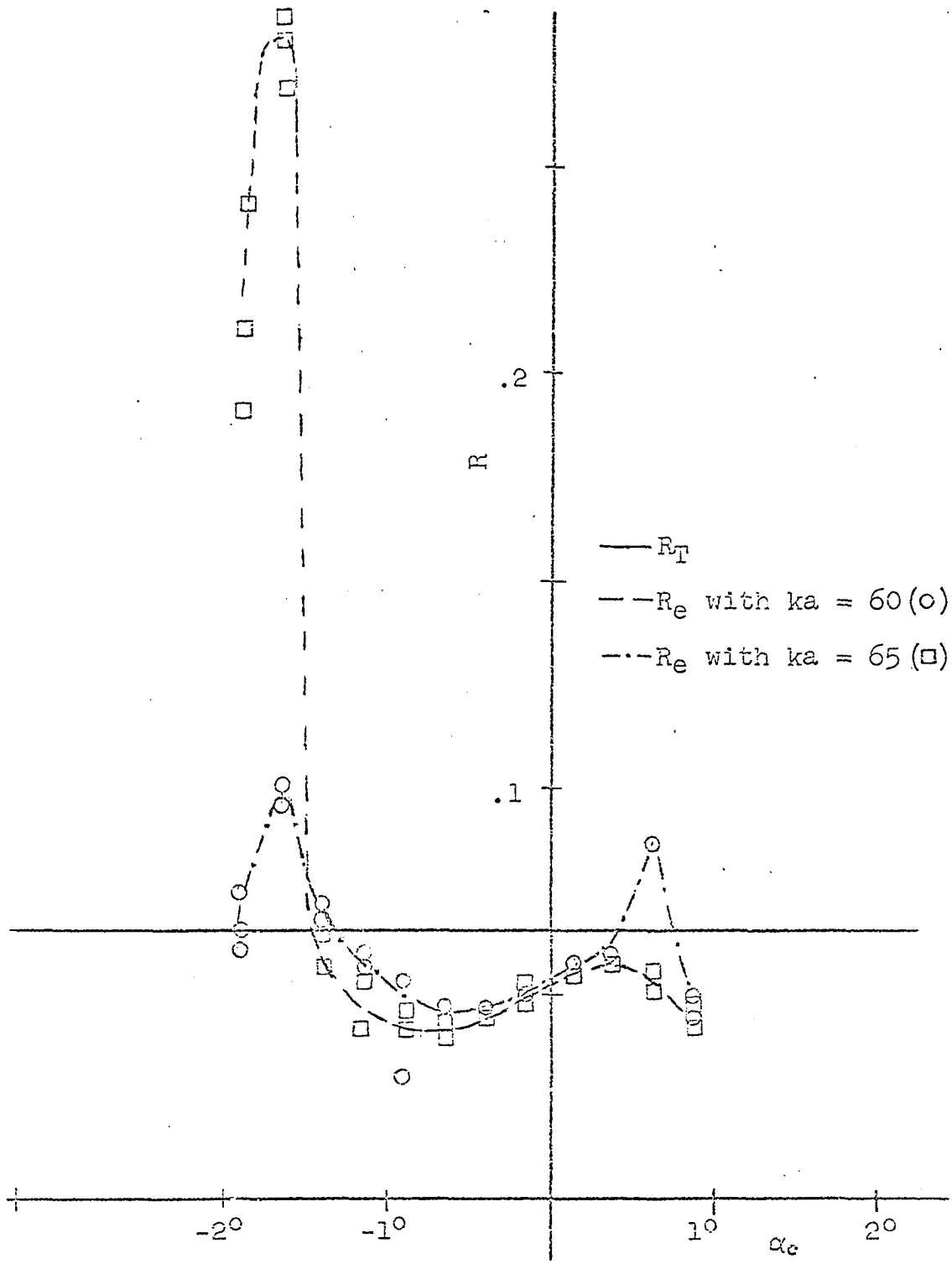


Figure 18. Graph showing $R_T$ and $R_e$ evaluated with $\beta = \delta/2r = 2^\circ$ and various ka. The reflecting surface was a water-polyethylene interface.